1973

Strength of composite beam-to-column connections, Nov. 1973

Dirk P. duPlessis

Hartley Daniels J.

STRENGTH OF COMPOSITE BEAM-TO-COLUMN CONNECTIONS

by

Dirk P. du Plessis

J. Hartley Daniels

This work has been carried out as part of an investigation sponsored by the American Iron and Steel Institute

Department of Civil Engineering
Fritz Engineering Laboratory
Lehigh University
Bethlehem, Pennsylvania

November 1973

Fritz Engineering Laboratory Report 374.3

TABLE OF CONTENTS

ABSTRACT

This report presents the results of an extensive investigation into the behavior of composite steel-conrete beam-to-column connections. The effect of seven test variables on the maximum strength, initial stiffness and ductility of the connections was studied. Sixteen composite beam-to-column connections were tested under positive moment (slab in compression) to investigate the seven test variables. Using the theory of plasticity upper and lower bounds for the maximum strength of the connections were established. Several conclusions are drawn of which the most important is that composite beam-to-column connections possess adequate rotation capacity to enable plastic design to be applied to unbraced frames with composite floor systems.

1. INTRODUCTION

The presence of floor systems rigidly connected to the beams of unbraced steel frames has long been known to increase the stiffness of such frames. A recent investigation into the behavior of an actual unbraced steel frame with composite precast concrete floor panels did show that such was the case.[1] It was therefore expected that the floor systems would have the same effect on the maximum strength of unbraced steel frames.

When an unbraced frame is subjected to lateral loads the columns apply end moments to the beams at the beam-to-column connections. If now the floor system is attached to the steel beams with shear connectors composite action results and the maximum strength and stiffness of the beams are increased. This increases the resistance to the applied end moments thereby increasing the maximum strength and stiffness of the beam-to-column connections and, as such, of the unbraced frame. It is therefore evident that composite beam-to-column connections can significantly affect the load-drift behavior of unbraced frames.

Reference 2 reports the first known study on the behavior of composite beam-to-column connections. Two composite beam-to-column connections representing typical interior and exterior connections of an unbraced frame were tested. Of particular interest was the behavior of the connection on the leeward side of the column where the composite beams are subjected to positive end moments (slab in compression).

Reference 3 reports the results of an investigation that con-

tinued the work reported in Ref. 2. Four composite beams were set-up to simulate the leeward side of composite beam-to-column connections. The test variables in that study were slab width and slab thickness. Of particular interest was the spalling and crushing pattern of the concrete at the column face. The test results showed that the maximum strength was independent of the slab width but was proportional to slab thickness. Correlation of the maximum strength of the connections with upper and lower bounds obtained from the theory of plasticity was good.

The behavior of composite beam-to-column connections in an unbraced frame is also influenced by other factors such as lateral beams framing into the column, shrinkage gaps between the column face and the concrete slab, formed metal deck slabs, connector spacing at the column, etc. These may all affect the maximum strength, stiffness and ductility of such connections. It was therefore considered necessary to further investigate the behavior of composite beam-to-column connections.

This report presents the results of an investigation to determine the effects of seven additional test variables on the behavior of composite beam-to-column connections under positive moment (slab in compression). The test variables are 1) a shrinkage gap between the column face and the concrete slab 2) shear connector spacing near the column face 3) concrete strength 4) steel beam depth 5) formed metal deck slabs 6) lateral beams framing into the column and 7) repeated loads. Of particular importance was the effect of these variables on the maximum strength, initial stiffness and ductility of the connections.

The experimental program consisted of the testing of eight com-

posite steel-concrete beams set up to simulate composite beam-to-column connections under positive moment (slab in compression). After one end of a composite beam was tested, the beam was turned around and the other end tested so that a total of sixteen tests were performed.

The theory presented in Ref. 3 to predict the behavior of composite beam-to-column connections was extended to suit the connections tested in this program. Experimental results were then compared with the theoretically predicted values.

This investigation is limited to composite beam-to-column connections using headed steel stud shear connectors. The effects of thickness and yield strength of the column flange were not investigated.

2. DESCRIPTION OF TESTS

2.1 Details of the Test Program

Details of the test program are shown in Table 1. The individual tests, designated A1, A2, B1, B2,----etc., were established on the basis of a two and three level partial factorial experiment design without replication to investigate the influence of six primary variables as follows:

Primary Variables:

1. Shrinkage gap size: Zero, 0.02 in
2. Shear connector density: High, Normal, Zero
3. Nominal concrete strength (f'_c): 3 ksi, 5 ksi
4. Steel beam depth: 12 in., 16 in.
5. Slab construction: Solid, Longitudinal metal deck, Transverse metal deck
6. Transverse support (lateral beams) at the column: With, Without
7. Repeated loads

Of the seven variables that were investigated the first six were explicitly incorporated into the factorial test program as shown in Table 1. The seventh was investigated only during tests A1 and A2.

All secondary variables were treated as one-level factors as follows:

One-Level Factors

1. Steel beam-to-column connection: Fully welded
2. Shear connectors: headed steel stud connectors
3. Steel beams: A572 Grade 50

4. Reinforcement: σ_y = 40 ksi (nominal)

5. Slab thickness: 4 in.

6. Concrete: Normal weight

The 0.02 in. shrinkage gap was determined on the basis of a shrinkage strain of 0.0002 over a span length of approximately 25 ft. between columns. This gives a value of 0.06 in. or 0.03 in. at each end of the span. In an actual structure the connectors would resist shrinkage so that 0.02 in. represents a liberal size.

Normal connector spacing meant that which is found in many typical buildings and was taken as 6 in. staggered based on calculations for a span length of approximately 25 ft between columns. Dense connector spacing implied connectors grouped considerably closer and zero spacing meant a complete absence of connectors.

The smaller value of nominal concrete strength (3 ksi) was considered typical of that found in many buildings. A difference of 2 ksi between the two concrete strengths was considered sufficient to show the effect of concrete strength.

Because the phase 1 test program[3] used 12 in. deep steel beams the same depth was adopted for this test program. This established a link between the two programs with the purpose of comparing test results.

As in the phase 1 test program a solid slab was retained for some of the tests. However, because of the increasing popularity of formed metal deck slabs, it was necessary to also investigate the latter.

All the phase 1 tests were performed without transverse support at the column. Since transverse support at a column is normally present in

any building it was considered appropriate to perform most of the tests with transverse support.

The one-level factors were selected on the basis of the results obtained in the phase 1 test program.[3]

2.2 Details of the Test Beams

2.2.1 Description

Figure 1 shows a schematic view of the test set-up. A 2 in. steel plate was welded to both ends of each steel beam to simulate the column face. During a test one steel plate was bolted to the column test fixture so that the test beam simulated a typical rigid composite beam-to-column building connection. After one end was tested, the test beam was turned around and the other steel plate bolted to the column test fixture. In this manner only 8 beams were required to obtain 16 connection tests.

Each test beam was bolted to the column test fixture with eight 1 in. diameter A490 bolts. The six bolts below the slab were required to resist the full yield force of the steel beam. All bolts were fastened using the turn-of-nut method.

Also shown in Fig. 1 are the four ½ in. diameter transverse support hangers that provide the transverse support at the columns. These hangers were suspended from the transverse beam on top of the column test fixture and supported the projections of the slab beyond the end plates.

Figure 2 shows a typical test beam. All the beams consisted of a 10'-8" x 4'-0" x 4" solid concrete or concrete on metal deck slab attached with 3 in long 3/4 in. diameter headed steel stud shear connectors to an 8 ft long A572 Grade 50 steel beam. The size of the steel

beam (W12 x 27) is the same as used for the phase 1 tests.[3]

Figures 3 and 4 show details of the test beams. The test corresponding to each end is also indicated. Beams A to D, G and H had a solid 4 in. concrete slab. Beam E had a 4 in. concrete slab on formed metal deck with ribs placed longitudinally to the steel beams. Beam F had a 4 in. concrete slab on formed metal deck with ribs running transverse to the steel beam. Beam H was the only beam with a W16 x 40 steel section.

Figure 5 shows details of the shear connector spacing. The variable connector spacing to provide the three levels of connector density was made within 15 in. of the steel plate as can be seen in the figure. This was done because the phase 1 tests showed that the spalled concrete never extended more than about 15 in. from the steel plate.[3] Outside these regions the connector spacing was determined by the total number of connectors required (see Section 2.2.2). Figures 6a and 6b show the typical normal and high density connector spacing in test beams with a solid slab. To obtain zero density no connectors were placed in the 15 in. region.

Figures 7a and 7b show details of the formed metal decking that was used on beams E and F respectively. It was anticipated that premature spalling would occur with the ribs in the transverse direction. For this reason a small area in front of the steel plates was flattened to provide full depth of concrete. This is shown in Fig. 7b. Figure 7c shows details of the geometry of the metal decking.

Figures 8a and 8b show the reinforcement details for the beams with solid slabs and metal decking respectively. Bar reinforcement was used for the solid slabs and welded wire mesh reinforcement was used

for the slabs with metal deck. Both types of slab had a double layer of reinforcement around the steel plates the purpose of which is explained in the next section.

2.2.2 Design

In the design of the shear connectors it was necessary to know the maximum compressive force which the steel plate would exert on the slab. This force was calculated using a concrete stress of 2.57 f'_c as obtained from Ref. 3. The connectors were then designed according to the AISC specification.[4]

In the design of the reinforcement for the slabs all the factors mentioned in Ref. 3 with regard to the design of slabs therein were included in this design. In addition, extra reinforcement was required to resist the bending moments caused by the projections of the slabs. The resultant accumulation of reinforcement at the steel plates is shown in Fig. 8. Because of the smaller strength of the metal deck slabs, the latter required less reinforcement than the solid slabs.

A 2 in. thickness was selected for the steel plates because of the satisfactory performance of the same plates during the previous test program.[3] The steel plates were of A36 steel partly because of easy availability at the time of construction and partly because the high strength plates used for the previous test program showed the possibility of delamination.

The 8 ft. length of the steel beam between the steel plates was selected on the basis of the results obtained from the previous test program.[3] After an examination of the yield pattern and concrete failure surfaces in Ref. 3, it was concluded that a length of 8 ft. would

be sufficient to prevent any significant interaction between the ends of the beam.

In the design of the transverse support hangers it was necessary to ensure that they would register sufficiently large strains, for purposes of accuracy, without yielding. After estimating the maximum force which each hanger would carry, an allowable stress of 26 ksi was used to determine the required diameter.

2.2.3 Construction

The steel beams were delivered to the laboratory with the 2 in. steel plates welded in position. Welding of the stud connectors was performed in the laboratory using standard stud welding equipment. The connectors for the beams with formed metal decking were welded to the steel beams through the decking as is standard practice.

For the beams which did not require a formed shrinkage gap at the steel plate the reinforcement running perpendicularly into the steel plate was welded to the plate. This is shown in Fig. 9a. It was assumed that this would prevent a large shrinkage gap at the steel plate. The same was done for similar beams with mesh reinforcement.

For the beams which did require a shrinkage gap at the steel plate a 0.02 in. plate was clamped to the steel plate before casting the concrete as shown in Fig. 9b. Approximately 3 hours after casting the concrete, this plate was removed and the top of the gap sealed to prevent dirt from entering.

Concreting for all the beams except beam G was performed using ready mixed concrete. Since only beam G required a concrete strength of

5000 psi it was decided to mix the concrete for this beam in the laboratory where strict control over mixing was possible. The beams were moist cured for seven days and then allowed to cure under dry conditions until the beams were tested.

2.2.4 Instrumentation

Figures 10a and 10b show the locations of the electrical resistance strain gages on the concrete slab and steel section of each test beam. The locations of gage lines B and C were determined considering the following restrictions:

1) A minimum distance of at least 4 in. from the steel plate was required to preclude the effect of local distortions.
2) A maximum distance of 15 in. from the steel plate was required to comply with the region of variable shear connector spacing (see Section 2.2.1).
3) No strain gages whould be placed directly below a shear connector on the steel beam.

Figure 11a shows the locations of electrical resistance strain gages on the transverse support hangers. This is also shown in Fig. 12a.

Figure 11b shows the locations of the Ames dial gages, electrical slip gages and rotation gages on a typical test beam. Ames dial gages measured the following:

1) Deflection at the applied load position
2) Uplift of the slab from the steel beam at the test location
3) Relative vertical slip between the steel plate and the test fixture
4) Horizontal deflection of the projections of the slab at the test location.

5) Closing of the shrinkage gap (if present) at the load position.

Relative horizontal slip between the slab and the beam was measured with the electrical slip gages at the test location. Level bar rotation gages measured the rotation of both steel plates and also the twisting of the test beam at the load position.

Figures 12b and 13a show the instrumentation at the test location and load position of a typical test beam.

2.2.5 Material Properties

Table 2 shows the mechanical properties of the steel beams. These were obtained by performing tensile tests on coupons cut from the control pieces left over from the rolled shapes used for the test beams. The coupons were tested in a 120 kip Tinius Olsen Universal machine at a speed of 0.025 in. per minute until fracture occurred. For all coupon tests the dynamic yield stress, the static yield stress and the maximum load were recorded.

Table 3 shows the mechanical properties of the stud connectors. These were obtained by performing tensile tests on stud connectors welded to a short length of the beam flange. Of the 5 connectors tested, one failed in the weld and the others failed by pulling out of the beam flange. The stud welds were also tested by welding some connectors to a short length of steel beam and bending them to a 45° angle. All welds proved satisfactory.

Table 4 shows the properties of the concrete obtained by crushing standard 6 in. diameter cylinders. In general, three cylinders were crushed before starting each of the two tests on every beam. The average of the six tests was assumed to represent the concrete strength

of both tests.

2.3 Test Set-up and Loading Procedure

The test set-up is shown in Fig. 1. Load was applied through a 60 ton mechanical jack bearing against a loading yoke which fitted around the steel plate. A 5/8 in. diameter bar welded to the bottom of the loading yoke provided a swivel point for the head of the jack. The mechanical jack rested on a calibrated load cell which was supported on a swivel base as shown in Fig. 13b.

The zero load position of a particular test beam was taken as the point at which there would theoretically be no moment at the steel plate at the test location. This required application of a small load equal to half the calculated beam weight. At this point the transverse support hangers were snugly tightened.

Loading proceeded in small increments until the mechanical jack ran out of stroke. At this stage some permanent deformation had normally already occurred. The beam was then unloaded and filler plates inserted between the swivel base and the load cell. Loading then continued until the jack again ran out of stroke. Normally at this point the maximum load had already been surpassed. The beam was then unloaded and the loose concrete at the end plate removed to inspect the failure surface.

Figures 14a and 14b show beam C before and after test C1. Figure 15a shows beam E (with the longitudinal ribs) in test position for test E1. Figure 15b shows beam F (with transverse ribs) at the end of test F1. These figures are representative of all the beams tested.

Beams A, B, G and H had a formed shrinkage gap at one end only.

In these cases the end without a shrinkage gap was tested first. This ensured that the steel plate at the load position did not affect the stiffness of the beam-to-column connection being tested.

Beam A was subjected to cyclic loading. For test A1 10 cycles from zero to approximately half the maximum load were perfomed. Test A2 was subjected to three series of cyclic loading as follows: 10 cycles from zero to approximately half the maximum load; 5 cycles from zero to approximately three quarters of the maximum load and 5 cycles at approximately the maximum load.

3. THEORETICAL ANALYSIS

The basis of the theoretical analysis required for the test beams was given in Ref. 3. It was shown therein that the theory of plasticity can be used to obtain upper and lower bounds for the maximum strength of the composite beam-to-column connections. Herein the work of Ref. 3 will be extended to cover the beams tested in this phase of the program.

3.1 Upper Bound Solution

Figure 16a shows the failure mechanism that was used to determine the upper bound for the connections without transverse support. The internal dissipation in this mechanism consists of the following parts:(3)

1) D_1 = internal dissipation in concrete wedge ABC
2) D_2 = internal dissipation due to shearing of slab along two vertical faces ABCF
3) D_3 = internal dissipation in steel beam web
4) D_4 = internal dissipation in bottom flange of steel beam
5) D_5 = internal dissipation in transverse reinforcement
6) D_6 = internal dissipation in longitudinal reinforcement
7) D_7 = internal dissipation in shear connectors

Figure 16b shows the corresponding failure mechanism for a connection with transverse support. There are two differences:

1) the additional plastic hinge in the projections of the slab
2) no shearing of slab along two vertical faces ABCF

The first difference implies an additional internal dissi-

pation equal to

$$D_8 = A_{sr} f_{yr} \left[t - \frac{A_{sr} f_{yr}}{2 f'_c (W - B)} - c_r \right] \quad (1)$$

where

A_{sr} = total area of reinforcement in bottom of slab

f_{yr} = yield stress of reinforcement

t = concrete slab thickness

f'_c = unconfined compressive strength of concrete

W = slab width

B = column width

c_r = concrete cover of reinforcement

The second difference implies that internal dissipation D_2 does not exist.

The upper bound value of the force P in Fig. 16b is then determined from the following equation:[3]

$$P_u = \frac{D_1 + D_3 + D_4 + D_5 + D_6 + D_7 + D_8}{L - t \cot \alpha} \quad (2)$$

where

L = span length

α = angle (Fig. 16b)

The corresponding upper bound moment M_u is

$$M_u = P_u L \quad (3)$$

3.2 Lower Bound Solution

Figure 17a shows the lower bound stress field assumed for connections without transverse support. This stress field differs from that reported in Ref. 3 in that the maximum concrete stress

was reduced from 2.57 f'_c to 1.30 f'_c. The 2.57 f'_c corresponds to a plane strain state of stress as given by the theory of plasticity.[3] Since the surface of the slab and regions close to it are obviously in a state of plane stress, it is inappropriate to use 2.57 f'_c over the full depth of the slab.

Reference 5 reports the results of 7.9" x 7.9" x 2" concrete specimens that were tested under biaxial compression. It was shown therein that a maximum concrete stress of approximately 1.3 f'_c could be attained in one direction if a compressive stress of about 0.4 f'_c was present in the second direction. In the case of a composite beam-to-column connection the concrete at the column is laterally confined by the projections of the slab. For this reason 1.3 f'_c was considered a suitable value for the lower bound stress field. However, since the concrete is further confined by the shear connectors and the top flange of the steel beam the stress field of Fig. 17a is an absolute lower bound for the maximum strength of a connection.

Figure 17b shows the lower bound stress field assumed for connections with transverse support. The only difference between Fig. 17a and 17b is the additional stress field in the projections of the slab. Since there is no lateral confinement in the projections the same maximum concrete stress of 0.85 f'_c as given by the AISC specification[4] for the design of composite beams was used in these regions.

4. PRESENTATION OF TEST RESULTS

4.1 Moment-Rotation Behavior

Figures 18 to 25 show the moment-rotation behavior of all the tests. The moment M at the column face has been nondimensionalized with respect to the plastic moment M_p of the steel section. The chord rotation θ has also been nondimensionalized with respect to the theoretical plastic hinge rotation θ_p of the steel beam, assuming a shape factor of 1. ($\theta_p = M_p L/3EI$).

Each figure also contains four theoretically predicted moment-rotation curves. Curves 1 and 2 are for the W12 x 27 or W16 x 40 steel section alone. Curve 1 assumes no strain hardening. Curve 2 includes strain hardening with a strain hardening modulus E_{st} = 550 ksi. Curve 3 is for a prismatic composite section consisting of the steel beam plus a slab width equal to the column face width. Similarly curve 4 is for a prismatic composite section consisting of the steel beam plus a slab width equal to the full slab width of the test beam.

The elastic slopes of all the curves were computed for prismatic beams having the same length as the test beams and loaded in the same manner. All the elastic slopes include the effects of flexure and shear deformation. Shear deformation was approximately equal to 10% of the flexural deformation.

The horizontal portion of curve 3 in Figs. 18 to 25 was determined using the lower bound stress fields of Fig. 17. The horizontal portion of curve 4 was obtained using the failure mechanisms of Fig. 16.

Specific developments which occurred during the loading procedure are also indicated in Figs. 18 to 25. These are:

Point A: cracking of the slab first observed

Point B: observed point of initiation of general yielding in the bottom flange.

Point C: spalling of the concrete slab adjacent to the steel plate.

Point D: the maximum moment

Point E: normal termination of a test. This occurred when unloading was evident due to concrete crushing or when very large rotations had been reached

Point F: termination of the test due to spreading of the crack in the tension flange of the steel beam

Point Y: first observed yielding in a small localized region in the tension flange directly below the cope hole in the web. Necking occurred almost simultaneously with the yielding. This was also the region where cracking of the flange finally occurred.

Figures 19 and 20 show the results obtained when the cracked bottom flanges of tests B2 and C1 were repaired with small flange plates welded to the steel beam. The flange plate of test B2 was considerably larger than that of test C1 causing the significant increase in moment capacity and flexural stiffness as can be seen in Fig. 19. The flange plate was added to test B2 after complete cracking of the tension flange had occurred. For test C1 the flange plate was added after partial

4.2 Failure Surfaces

Figures 26 and 27 show typical failure surfaces in the concrete slab at the column face at the end of testing. The crushing and spalling of the concrete exposed the metal decking of beams E and F as shown in Fig. 27. This implies that at the end of the test the composite section for these beams in the vicinity of the column face was essentially that of the steel beam alone.

Figure 28 shows the yielding and cracking patterns for tests G1 and F2. For test G1 the steel beam yielded mainly in tension as can be seen in Fig. 28a. Figure 28b shows that compression yielding occurred in the upper part of the steel beam of test F2. Local buckling of the compression flange of test F2 also can be seen. It can be further observed that the local buckling and the concrete rib that had failed are both located near the end of the flattened region of the metal deck (Art. 2.2.1.)

4.3 Description of Tension Flange Cracking

Figure 29 shows two different kinds of cracking in the heat affected zone of the tension flange. For the connections with a W12 x 27 steel section the cracking initiated below the cope hole in the web and slowly spread outwards as shown in Fig. 29a. This figure also shows the yielding that occurred in the vicinity of the crack. Considerable necking was also visible.

Figure 29b shows the cracking that occurred in both tests with the W16 x 40 steel section (test H1 and H2). The cracking occurred suddenly, with a loud report, and completely severed the flanges. The cracks displayed a brittle surface with no significant necking or yielding.

4.4 Forces in the Transverse Support Hangers

Figures 30 and 31 show the forces that developed in the transverse support hangers of test C2 and E1 respectively. The tension forces are plotted against the nondimensionalized moment M/M_p at the column face. Points A, B and C in Figs. 30 and 31 correspond to the same points in Figs. 18 to 25. It is evident from Figs. 30 and 31 that the two interior bars carry essentially the total load.

Also plotted in these figures is the ratio M_s/M versus M/M_p where M_s is the moment applied at the steel plate by all four transverse support hangers and M is the total applied moment at the steel plate. The ratio M_s/M always remains quite small. It initially decreases but later increases rapidly when spalling of the concrete begins at the steel plate.

4.5 Slip between Slab and Steel Beam

Figure 32 shows the relative slip between the slab and the steel beam at gage section B (Fig. 10) for test beams A and B. Positive and negative values of slip imply movements of the concrete slab away and towards the steel plate respectively. Tests A1 and B1 were without shrinkage gaps. While tests A2 and B2 were with shrinkage gaps. Points A, B and C in Fig. 32 correspond to the same points in Figs. 18 to 25. It is evident that the effect of a shrinkage gap is to cause a large negative slip relative to that caused by a beam with no shrinkage gap.

5. EVALUATION OF TEST RESULTS AND DISCUSSION

5.1 Parameters

The effect of each of the seven test variables listed in Chapter 1 will be investigated in the light of the following three parameters:

1) Maximum Strength Ratio: - the maximum value of the M/M_p ratio as obtained from the moment -- rotation curves in Figs. 18 to 25.

2) Initial Stiffness: - the initial slope of the moment-rotation curves in Figs. 18 to 25 computed between the start and the end of the first load increment.

3) Ductility Factor: - the definition of ductility given in Ref. 6 will be used. Ductility is defined there as the ability of a structure to undergo increasing deformation beyond the initial yield deformation while still sustaining load. Consider the typical moment-rotation curve in Fig. 33. Point B is the initial yield rotation "a" and point D is the peak rotation "b". A measure of ductility is the ductility factor defined by[6]

$$\text{Ductility factor} = \frac{\text{Peak rotation}}{\text{Yield rotation}} = \frac{b}{a} \qquad (4)$$

Table 5 presents the maximum strength ratio, initial stiffness and ductility factor for each of the tests. The lowest values of maximum strength (1.54-1.61) correspond to tests E1, E2, F1 and F2 which had the formed metal deck slabs. The highest value (1.87) corresponds to test G1 which had a solid slab and the highest concrete strength as can be seen from Table 4. It is significant to note in Fig. 24 that test G2 had a comparatively early flange rupture. This fact should be considered when noting the maximum strength ratio for test G2.

The formed shrinkage gaps in tests A2, B2, D1, D2, G2 and H2 were not all exactly the same size because of the method of constructing the gaps. In addition those tests which did not require formed shrinkage gaps were observed to have a small natural shrinkage gap between the steel plate and the slab. This was especially noticeable with beams E and F probably because the smaller amount of reinforcement in the metal deck slabs was insufficient to prevent shrinkage. The above factors must be considered when comparing initial stiffnesses in Table 5. Other factors which may have had small influences on the initial stiffness are the amount of concrete that was destroyed during testing of the other end of the beam and whether or not a formed shrinkage gap was present at the other end.

The minimum ductility factor achieved was 4.4 for test G2. This value may have been affected by the comparatively early flange cracking as was mentioned earlier.

In Tables 6 to 12 the effects of the 7 test variables listed in Chapter 1 are investigated. In each of these tables "increase" implies an increase of the value of the parameter (maximum strength ratio, initial stiffness or ductility factor) corresponding to the test listed in Column 1 over that of the test listed in Column 2. The percentage increase or decrease is calculated on the basis of the value associated with the test in Column 2.

5.2 Effect of a Shrinkage Gap

Referring to Table 1 it can be seen that the only difference between tests A1 and A2, B1 and B2, G1 and G2 and H1 and H2 was the presence of a formed shrinkage gap. The results of these tests there-

fore will enable the effect of a shrinkage gap to be isolated.

1) Maximum Strength Ratio

In Table 6 the variation in maximum strength ratio between the tests with and without formed shrinkage gaps are shown. The large decrease in M_{max}/M_p between tests G1 and G2 is probably due to the relatively early cracking of the bottom flange of test G2 (Section 5.1) This decrease is therefore unreliable and should be ignored. The average change in maximum strength ratio (ignoring test G2) is a decrease of 1.0 percent. Such a small change indicates that a shrinkage gap has a negligible effect on the maximum strength of a composite beam-to-column connection.

This result can be explained with the aid of Fig. 34a which shows the column in contact with the slab after the shrinkage gap has closed. Because of the inclination of the beam the concrete in contact with the column is in a three dimensional state of stress. It is known that under such a state of stress concrete strength increases greatly. Therefore, even though the lower part of the slab may still be separated from the column face the increased strength of the concrete in the upper part is sufficient for the connection to reach nearly the same strength as in the case without a shrinkage gap.

2) Initial Stiffness

Table 6 shows that there is a large decrease in the initial stiffness when a shrinkage gap is present. This can be explained with the aid of Fig. 34b. While the slab is still separated from the column face the length of noncomposite action is the distance from the column face to the first row of connectors. Because this noncomposite action occurs in a region of maximum bending moment it results in a substantial decrease in initial stiffness.

3) Ductility Factor

Table 6 shows that there is a definite decrease in the ductility factor when a shrinkage gap is present. This decrease can be attributed to several reasons, as follows:

a) The decrease in initial stiffness mentioned earlier causes yielding to occur at a greater rotation. This can be seen in Figs. 22, 24 and 25. The value of the yield rotation "a" in Fig. 33 is therefore larger, leading to a decrease in the ductility factor.

b) The greater concrete strength under a three dimensional state of stress near the column face may result in the connection reaching its maximum strength more rapidly after the shrinkage gap closes. This could be the reason why tests A2 and B2 reached their maximum strength at a smaller rotation than tests A1 and B1 respectively (Figs. 18 and 19). This causes the peak rotation "b" in Fig. 33 to be smaller leading also to a decrease in the ductility factor.

5.3 Effect of Connector Density

Comparing tests C1 and C2, D1 and D2, E1 and E2, F1 and F2 in Table 1 shows that the only variable in these tests is connector density. The results of these test will therefore indicate the effect of connector density.

1) Maximum Strength Ratio

Table 7 shows that there is no definite trend in the variation of maximum strength between the pertinent tests. In addition the actual values of percentage decrease or increase are comparatively small. This result can be explained as follows. The connectors in the immediate vicinity of the column contribute little to the total transfer of shear between slab and beam. Their density in front of the column is therefore

not expected to influence the maximum strength of the connections as long as there are sufficient connectors along the beam to develop the maximum concrete force or the yield force of the steel beam whichever is less.

2) Initial Stiffness

Table 7 indicates a small reduction in initial stiffness with a decrease in connector density. The largest reduction occurred between tests E1 and E2. When E1 was tested the opposite end (E2) had not yet been tested. Upon testing E2 very little concrete was present at E1 as can be seen in Fig. 27a. This could have contributed to the decrease in initial stiffness of test E2.

The average decrease in initial stiffness is comparatively small and does not indicate a definite trend. It should therefore be concluded that connector density at the column does not significantly affect the initial stiffness of a composite connection. The initial stiffness is more dependent on the total number of connectors provided along the length of the beam.

3) Ductility Factor

Table 7 shows that there is an increase in the ductility factor with a decrease in connector density at the column. This increase is contrary to what was expected. It has been found that the ductility of reinforced concrete increases with an increase in the number of stirrups.[7,8] It was therefore expected that an increase in connector density should lead to an increase in ductility.

The connectors close to the column are largely responsible for resisting uplift of the slab when lateral support at the column is present. Increasing the connector density in this region would therefore decrease uplift and consequently increase the curvature of the slab as

shown in Figs. 35a and b. The increased curvature causes a higher compressive stress in the upper part of the slab for the same applied load. This could result in an earlier attainment of the maximum strength ratio (tests E1 and F1 versus E2 and F2) with a consequent decrease in the ductility factor as was explained in Section 5.2.

It is therefore concluded that an increase in connector density at the column could lead to a decrease in the ductility factor.

5.4 Effect of Concrete Strength

Table 1 shows that the effect of concrete strength can be determined by comparing tests G1 and G2 with C1 and D1 respectively. Because it was shown in Section 5.3 that connector density does not affect either maximum strength ratio or initial stiffness, tests G1 and G2 can also be compared with A1, A2, C2 and D2. However, the comparatively early flange cracking of G2 (Section 5.1) makes comparisons with this test unreliable and, therefore, only the results of test G1 will be used.

1) Maximum Strength Ratio

Table 8 shows that an increase in concrete strength leads to an increase in maximum strength ratio as can be expected. This is because, as the concrete strength increases, the contribution of the slab to the maximum strength of the connection increases. However, whereas there was nearly a 50 to 70 percent increase in concrete strength (see Table 4) the average increase in maximum strength ratio was only 8.7 percent as shown in Table 8.

2) Initial Stiffness

Table 8 shows a small increase in initial stiffness with an

increase in concrete strength. The modulus of elasticity of concrete is proportional to its compressive strength and an increase in the latter, therefore, increases the moment of inertia of the cross section causing an increase in initial stiffness. Again the increase in initial stiffness (3.6%) is small in comparison with the increase in concrete strength (50%).

3) Ductility Factor

As shown in Table 8 there is a definite decrease of the ductility factor with an increase in concrete strength. This may be due to the following reasons:

a) An increased concrete strength may cause the connections to attain their maximum strength more rapidly and therefore decrease the peak rotation "b" in Fig. 33. This can clearly be seen when the peak rotation of test G1 is compared with those of tests A1, C1 and C2. The ductility factor will therefore be smaller.

b) Increasing the concrete strength raises the neutral axis which retards initial yielding of the bottom flange. This would increase the initial yield rotation "a" in Fig. 33 and therefore decrease the ductility factor.

5.5 Effect of Steel Beam Depth

A comparison of tests H1 and H2 with C1 and D1 in Table 5 shows that these tests differed only in the size of the steel beam. There was, however, also a difference in concrete strength as shown in Table 4 which should be considered when comparing test results. Since it was shown in Section 5.3 that connector density does not affect either the maximum

strength ratio or the initial stiffness tests H1 and H2 can also be compared with A1, A2, C2 and D2.

1) Maximum Strength Ratio

Table 9 shows a consistent decrease in maximum strength ratio with an increase in beam depth. Increasing the beam depth increases the contribution of the steel beam to the maximum strength of the connection thereby decreasing the maximum strength ratio.

2) Initial Stiffness

Table 9 indicates that the initial stiffness is decreased when the beam depth increases. The reason for this result may be the following. Because of the greater beam size the shear connectors of beam H transmitted a much greater shear force than those of beams A, C and D. Since all these beams had practically the same total number of shear connectors as can be seen in Fig. 5 the connector slip in test H1 and H2 was greater than that in tests A1, A2, C1, C2, D1 and D2. This would have caused a decrease in the initial stiffness of H1 and H2.

3) Ductility Factor

Table 9 shows that there is a small average increase in the ductility factor with an increase in beam depth. There is however no definite trend and it should be concluded that beam depth has a negligible effect on the ductility of a composite beam-to-column connection.

5.6 Effect of Formed Metal Deck Slabs

Tests E1, E2, F1 and F2 differed from tests A1, C1 and C2 in the following way:

a) metal deck slabs versus solid slabs (Table 1)

b) arrangement of connectors near the steel plates (Fig. 5)

c) concrete strengths (Table 4)

d) small changes in yield strength of the steel beam (Table 2).

The small differences in yield strength can be ignored. Knowing the effects of connector density and concrete strength from Sections 5.3 and 5.4 the above named tests can be compared to determine the effect of metal deck slabs.

1) Maximum Strength Ratio

Tables 10 and 11 show that the maximum strength ratio decreases when metal deck slabs are used. This can be expected because of the lesser amount of concrete in metal deck slabs. The tables also show that the decrease in maximum strength ratio is approximately the same regardless of the direction of the ribs. However, had it not been for the flattened transverse ribs at the steel plate (Fig. 7b) tests F1 and F2 may have exhibited a greater decrease in maximum strength ratio.

2) Initial Stiffness

There is a substantial decrease in initial stiffness when formed metal deck slabs are used as can be seen in Tables 10 and 11. Part of this decrease is due to the lesser amount of concrete in the metal deck slabs. The major reason however for the significant decrease in initial stiffness is probably the presence of natural shrinkage gaps in tests E1 and F1 as was mentioned in Section 5.1. Had this not been the case the decreases in initial stiffness would probably not have been as large.

The tables also show that the orientation of the ribs did not play a significant role in decreasing the initial stiffness. This is

most likely due to the proximity of the concrete in the ribs to the neutral axis of the composite beam.

3) Ductility Factor

Tables 10 and 11 show that there is a decrease in the ductility factor when formed metal deck slabs are used. The reason for this is probably twofold:

a) The concrete at the column is less confined because of the absence of concrete between the ribs and is therefore less ductile.[7,8] This may decrease the ductility factor.

b) Figures 18, 20, 22 and 23 show that the peak rotations of tests E1, F1 and F2 is smaller than those of A1, C1 and C2. The ductility factor which is proportional to the peak rotation (Section 5.1) would therefore also be smaller.

Tables 10 and 11 also indicate a greater decrease in the ductility factor with transverse ribs than with longitudinal ribs. Figures 22 and 23 show that the peak rotations of tests F1 and F2 were smaller than that of test E2. This could have caused the additional decrease in ductility factor for tests F1 and F2.

5.7 Effect of Lateral Support at the Column

The effect of lateral beams can be determined by comparing tests B1 and B2 with C1 and D1 as shown in Table 1. Because of the differences in concrete strength as shown in Table 4 the above comparison would yield inaccurate results. Since it was shown in Section 5.3 that connector density does not influence maximum strength ratio or initial stiffness a better comparison would be between tests B1 and A1 and B2 and A2.

1) Maximum Strength Ratio

Table 12 shows a small increase in maximum strength ratio in the presence of lateral support. The lateral support forces the projections (the portions of the slab on the sides of the column) into bending thereby increasing the moment resistance of the connection. The increase in maximum strength ratio is most likely a function of the slab width, amount of reinforcement and yield stress of the reinforcement.

2) Initial Stiffness

Lateral support at the column increases the initial stiffness of the connection as shown in Table 12. As a result of the action of the lateral support as explained above the moment of inertia of the composite section at the column is increased by that of the projections. This results in an increase in the initial stiffness of the connection. The increase in initial stiffness is again a function of the slab width.

3) Ductility Factor

Table 12 shows a small decrease in the ductility factor in the presence of lateral support. There is however no definite trend and because the decrease is relatively small it is concluded that lateral support at the column has no significant effect on the ductility factor.

5.8 Effect of Repeated Loads

The effect of repeated loads was investigated during the execution of tests A1 and A2 (Section 2.1). Since no significant changes were observed it can be concluded that repeated loads have no appreciable effect on either maximum strength ratio, initial stiffness or ductility factor.

Table 13 summarizes the test results of this experimental study.

5.9 Correlation with Theoretical Analysis

Table 14 shows a correlation of the test values of the maximum strength ratio with the upper and lower bound values. Except for test G2 all the test values exceeded or at least equalled the lower bound values. The reason for test G2 not reaching the lower bound is due to the comparatively early flange cracking (Section 5.1). It can therefore be concluded that the lower bound stress field of Fig. 17a or 17b is a true lower bound.

Table 14 also shows that none of the test values exceeded the upper bounds. The test values of the maximum strength ratio were thus effectively bounded by the upper and lower bounds obtained from Ch. 3.

Table 15 shows a break-down of the internal dissipation in the upper bound mechanism (Section 3.1) as obtained for each of the tests. The values in column 7 represent the contribution by the shear connectors. Since these values constitute a comparatively small part of the total internal dissipation the shear connectors do not significantly affect the maximum strength of the connections. This observation supports the conclusion reached in Section 5.3.

A survey of Figs. 18 to 25 show that the initial stiffness of the tests without a shrinkage gap is well approximated by that of curve 3. The initial stiffness of the tests with a shrinkage gap lies between that of curves 1 and 3. Frame behavior in the presence of shrinkage gaps is currently being investigated in Ref. 9.

5.10 Application to Analysis and Design of Unbraced Frames with Composite Beams

5.10.1 Maximum Strength

Table 16 shows the ratio of maximum strength over lower bound value for all the tests performed to date. The lower bound values were

obtained from the stress field of Fig. 17b. It is therefore concluded that Fig. 17b provides a good lower bound for the maximum strength of a composite beam-to-column connection under positive moment.

Figure 36 shows a plan of an unbraced frame with composite beams. At the leeward side of the columns the stress field of Fig. 17b applies using 1.30 f'_c for the concrete in contact with the columns. At some distance L_t from the columns the maximum strength of the composite section can be determined using 0.85 f'_c for the concrete[4]. Within this transition length (L_t) the concrete strength on which maximum strength calculations should be based, is unknown. This problem is being investigated.

5.10.2 Initial Stiffness

An extensive study is being conducted to determine what uniform stiffness should be assigned to the composite beams so that the unbraced frame with these beams will have the same stiffness as with the full panel width floors.[9]

5.10.3 Ductility

Table 5 shows that the minimum ductility factor achieved was 4.4. Reference 6 indicates that for buildings in earthquake areas a ductility factor between 4 and 6 is recommended. It can therefore be concluded that from this point of view all the connections exhibited adequate ductility.

In plastic design of steel structures rotation capacity is defined as the angular rotation which a given cross-sectional shape can accept at the plastic moment value without prior local failure.[10,11] Rotation capacity is indicated in Fig. 37. Assuming that this definition also

applies to composite connections and taking the plastic moment M_p as the lower bound value (curve 3 in Figs. 18 to 25) then the rotation capcity of each test is as shown in Table 17. It has been found that in many unbraced steel frames the required rotation capcity is of the order of the deflection index at maximum load. Assuming a typical deflection index of less than 0.02 at maximum load it can be seen that all the tests except G2 had adequate rotation capacity.

Curve H2 in Fig. 25 needs further discussion. It appears as if this test had inadequate rotation capacity since a very large rotation was necessary to reach the lower bound value. Comparing curves H2 and H1 it will be seen that this behavior was due to a more rapid reduction in stiffness and not due to inadequate ductility.

It is therefore concluded that plastic design can be applied to unbraced frames with composite beams.

6. SUMMARY AND CONCLUSIONS

A series of tests was performed to investigate the effect of seven primary variables on the behavior of composite steel-concrete beam-to-column connections. The primary variables were 1) a shrinkage gap between the column face and the concrete slab; 2) shear connector spacing near the column face; 3) concrete strength; 4) steel beam depth; 5) formed metal deck slabs; 6) lateral beams framing into the column and 7) repeated loads. Of particular importance was the effect of the test variables on the maximum strength, initial stiffness and ductility of the connections.

The test program comprised a two and three level partial factorial experiment design without replication. Sixteen tests were performed to investigate the seven primary variables. All secondary variables such as the yield strength of the steel beams, the slab thickness and the type of shear connectors were treated as one level factors.

The experimental program consisted of the testing of eight composite steel-concrete beams. Each beam in turn was bolted to a rigid column test fixture to form a cantilever. With the aid of a mechanical jack an upward load was applied at the free end of the beam. This caused the concrete at the column end of the beam to go into compression thus simulating the leeward side of a composite beam-to-column connection. Loading of the connection continued until either the deflection became too large or the bottom flange of the steel beam cracked. The beam was then turned around and the other end bolted to the column test fixture. In this manner eight beams were used to obtain sixteen tests.

The maximum strengths of the connections were compared with

upper and lower bound values obtained from the theory of plasticity. For the upper bound value a failure mechanism was assumed and the total internal dissipation then minimized. For the lower bound value a statically admissible stress field was assumed at the column face. All the test values of the maximum strength lay between the upper and lower bound values.

Based on the test results several conclusions may be drawn:

1) The maximum strength of a composite beam-to-column connection using solid slab construction can exceed the maximum strength of the bare steel connection by 64 to 87%.
2) A shrinkage gap between the column face and concrete slab causes a significant decrease in the initial stiffness of a connection but has no effect on the maximum strength. Ductility is slightly decreased.
3) Connector density at the column face has no appreciable effect on either maximum strength or initial stiffness of a connection. Increasing the connector density may reduce the ductility of the connection.
4) Increased concrete strength results in an increase in maximum strength and initial stiffness of a connection but may reduce the ductility.
5) Increasing the size of the steel beam increases the maximum strength and inital stiffness but has no appreciable effect on ductility of a composite connection.
6) The maximum strength of a composite beam-to-column connection using formed metal deck slab construction can exceed the maximum strength of the bare steel connection by 54 to 61%.
7) Lateral beams framing into the column increases the maximum strength and initial stiffness of a composite beam-to-column connection but has no appreciable effect on ductility.

8) Repeated service loads have no significant effect on either maximum strength, initial stiffness or ductility of a connection.

9) A good lower bound for the maximum strength of a composite beam-to-column connection can be obtained by using a concrete stress of $1.3\ f'_c$ over a width equal to the column face width.

10) Composite beam-to-column connections possess adequate rotation capacity to enable plastic design to be applied to unbraced frames with composite steel-concrete floor systems.

7. ACKNOWLEDGMENTS

The investigation described herein was conducted at Fritz Engineering Laboratory, Lehigh University, Behtlehem, Pa. Dr. Lynn S. Beedle is Director of the Laboratory and Dr. David A. VanHorn is Chairman of the Department of Civil Engineering.

The authors wish to thank the Committee of Structural Steel Producers and the Committee of Steel Plate Producers of the American Iron and Steel Institute for sponsoring this research. The contribution of the AISI Task Force on Project 173 consisting of Dr. W. C. Hansell as Project Supervisor and Professor E. H. Gaylord, Messrs. A. C. Hauswald, H. S. Lew and W. A. Milek, Jr. is gratefully acknowledged.

The authors gratefully ackowledge the assistance given by Mr. Ken Harpel, Laboratory Superintendant, and his staff in preparing the test set-ups. The manuscript was carefully typed by the staff of Ms. D. Ritter and the figures were prepared by Mr. John Gera and Ms. Sharon Balogh.

8. NOMENCLATURE

A_{sr}	=	total area of reinforcement in bottom of slab
A_s	=	total area of steel beam
B	=	width of steel plate or column
D	=	internal dissipation of energy
L	=	length of test beam
M	=	end moment of test beam
M_p	=	plastic moment of steel beam
M_s	=	total moment at the steel plate applied by transverse support hangers
P	=	applied vertical force at free end of test beam
W	=	slab width
c_r	=	concrete cover of the reinforcement
d	=	total depth of the steel beam
f'_c	=	cylinder compressive strength of concrete
f_y	=	average yield stress of steel beam
f_{yr}	=	yield stress of reinforcement
f_{yw}	=	yield stress of steel beam web
t	=	slab thickness
t_w	=	thickness of beam web
α	=	angle
θ	=	angular velocity
θ_p	=	rotation corresponding to plastic moment of steel beam

		SERIES 1			SERIES 2					
		W12x27 f'_c=3ksi			W12x27 f'_c=3ksi					
		4" Solid Slab			4" Longitudinal Metal Deck			4" Transverse Metal Deck		
	Gap Size (in)	Connector Density			Connector Density			Connector Density		
		High	Normal	Zero	High	Normal	Zero	High	Normal	Zero
With Transverse Support Hangers	0	C1	A1	C2	E1	E2		F1	F2	
	0.02	D1	A2	D2						
Without Transverse Support Hangers	0	B1								
	0.02	B2								

		SERIES 3			SERIES 4		
		W12x27 f'_c=5ksi			W16x40 f'_c=3ksi		
		4" Solid Slab			4" Solid Slab		
	Gap Size (in)	Connector Density			Connector Denisty		
		High	Normal	Zero	High	Normal	Zero
With Transverse Support Hangers	0	G1			H1		
	0.02	G2			H2		
Without Transverse Support Hangers	0						
	0.02						

Note: All values of f'_c shown are nominal values.

Table 1: DETAILS OF THE TEST PROGRAM

SHAPE	BEAM NUMBER	PART	DYNAMIC YIELD STRESS (KSI)		STATIC YIELD STRESS (KSI)		TENSILE STRENGTH (KSI)	
			TEST	AVERAGE	TEST	AVERAGE	TEST	AVERAGE
W12x27	A B C D	FLANGE	57.4 57.6 56.7 57.5	57.3	55.2 55.6 54.3 55.0	55.0	77.8 77.8 77.0 77.8	77.6
		WEB	59.8 61.2	60.5	57.9 59.4	58.7	82.3 82.8	82.5
	E F G	FLANGE	56.4 56.4 56.6 56.8	56.5	54.9 54.3 53.7 54.0	54.2	77.7 77.2 77.0 77.0	77.2
		WEB	58.0 58.1	58.1	55.8 55.4	55.6	78.6 79.7	79.2
W16x40	H	FLANGE	57.4 57.2 57.0 57.5	57.3	55.3 54.8 55.1 54.6	55.0	82.4 83.0 82.4 83.2	82.8
		WEB	58.6 60.7	59.7	56.6	56.6	81.3 81.7	81.5

Table 2: MECHANICAL PROPERTIES OF STEEL BEAMS

LENGTH (in)	DIAMETER (in)	TENSILE STRENGTH (KSI)		PERCENTAGE ELONGATION	
		TEST	AVERAGE	TEST	AVERAGE
3	3/4	67.5 68.8 74.5 66.8 70.4	69.5	----	----

Table 3: MECHANICAL PROPERTIES OF STUD CONNECTORS

BEAM NUMBER	COMPRESSIVE STRENGTH (KSI)		SLUMP (IN)	AVERAGE MODULUS OF ELASTICITY (KSI)
	TEST	AVERAGE		$57\sqrt{f'_c}$
A1, A2	3.45 3.34	3.40	4½	3330
B1, B2	3.57 3.53	3.55	4½	3400
C1, C2	4.44 4.54 4.44 4.40 4.62 4.51	4.49	6¼	3820
D1, D2	4.52 4.67 4.51 4.47 4.60 4.59	4.56	—	3850
E1, E2	4.05 4.19 4.26 4.08 4.25 4.32	4.19	—	3690
F1, F2	4.11 4.30 4.37 4.20 4.15 4.08	4.20	—	3700
G1, G2	6.26 6.08 6.13 6.14 6.28 6.03	6.15	—	4480
H1, H2	3.70 3.84 3.59 3.77 3.77 3.77	3.74	—	3480

Table 4: PROPERTIES OF THE CONCRETE

TEST NUMBER	MAXIMUM STRENGTH RATIO M_{MAX}/M_p	INITIAL STIFFNESS	DUCTILITY FACTOR
A1	1.73	1.80	7.8
A2	1.68	1.25	5.6
B1	1.64	1.73	7.5
B2	1.65	1.23	6.4
C1	1.72	1.67	4.8
C2	1.71	1.69	5.0
D1	1.75	1.27	5.9
D2	1.79	1.21	6.3
E1	1.59	1.47	4.6
E2	1.54	1.27	5.7
F1	1.57	1.30	4.6
F2	1.61	1.31	4.8
G1	1.87	1.78	4.7
G2	(1.65)	1.45	(4.4)
H1	1.68	1.67	6.4
H2	1.67	1.00	5.6

Table 5: MAXIMUM STRENGTH, INITIAL SLOPE AND DUCTILITY FACTORS

EFFECT OF A SHRINKAGE GAP							
TESTS (WITH SHRINKAGE GAP)	TESTS (WITHOUT SHRINKAGE GAP)	MAXIMUM STRENGTH RATIO M_{MAX}/M_p		INITIAL STIFFNESS		DUCTILITY FACTOR	
1	2	INCREASE %	DECREASE %	INCREASE %	DECREASE %	INCREASE %	DECREASE %
A2	A1		2.8		30.5		28.2
B2	B1	0.6			28.9		14.7
G2	G1		(11.8)		18.5		(6.4)
H2	H1		0.7		40.0		12.5
AVERAGE			1.0		29.5		18.5

Table 6: Effect of a Shrinkage Gap

EFFECT OF CONNECTOR DENSITY							
TESTS (LESS DENSE SPACING)	TESTS (DENSER SPACING)	MAXIMUM STRENGTH RATIO M_{MAX}/M_p		INITIAL STIFFNESS		DUCTILITY FACTOR	
1	2	INCREASE %	DECREASE %	INCREASE %	DECREASE %	INCREASE %	DECREASE %
C2	C1		0.6	1.2		4.2	
D2	D1	2.3			4.7	6.8	
E2	E1		3.1		13.6	24.0	
F2	F1	2.5		0.8		4.3	
AVERAGE		0.3			4.1	9.8	

Table 7: Effect of Connector Density

EFFECT OF CONCRETE STRENGTH							
TESTS (HIGH CONCRETE STRENGTH)	TESTS (NORMAL CONCRETE STRENGTH	MAXIMUM STRENGTH RATIO		INITIAL STIFFNESS		DUCTILITY FACTOR	
		INCREASE %	DECREASE %	INCREASE %	DECREASE %	INCREASE %	DECREASE %
1	2						
G1	A1	8.1			1.1		39.1
G1	C1	8.7		6.6			2.1
G1	C2	9.3		5.3			6.0
AVERAGE		8.7		3.6			15.9

Table 8: Effect of Concrete Strength

EFFECT OF STEEL BEAM DEPTH							
TESTS (LARGER BEAM DEPTH)	TESTS (SMALLER BEAM DEPTH)	MAXIMUM STRENGTH RATIO		INITIAL STIFFNESS		DUCTILITY FACTOR	
		INCREASE %	DECREASE %	INCREASE %	DECREASE %	INCREASE %	DECREASE %
1	2						
H1	A1		2.9		7.2		18.0
H1	C1		2.3		0.0	33.3	
H1	C2		1.8		1.2	38.0	
H2	A2		0.6		20.0		0.0
H2	D1		4.6		21.3		5.1
H2	D2		6.7		17.4		11.1
AVERAGE			3.1		11.2	4.5	

Table 9: Effect of Steel Beam Depth

EFFECT OF METAL DECK SLABS: LONGITUDINAL RIBS							
TESTS (WITH METAL DECK SLABS)	TESTS (WITH SOLID SLABS)	MAXIMUM STRENGTH RATIO		INITIAL STIFFNESS		DUCTILITY FACTOR	
		INCREASE %	DECREASE %	INCREASE %	DECREASE %	INCREASE %	DECREASE %
1	2						
E1	A1		8.1		18.3		41.0
E1	C1		7.6		12.0		4.2
E1	C2		7.0		13.0		8.0
E2	A1		11.0		29.4		26.9
E2	C1		10.5		24.0	18.7	
E2	C2		9.9		24.9	14.0	
AVERAGE			9.0		20.3		7.9

Table 10: Effect of Metal Deck Slabs with Longitudinal Ribs

EFFECT OF METAL DECK SLABS: TRANSVERSE RIBS							
TESTS (WITH METAL DECK SLABS)	TESTS (WITH SOLID SLABS	MAXIMUM STRENGTH RATIO		INITIAL STIFFNESS		DUCTILITY FACTOR	
		INCREASE %	DECREASE %	INCREASE %	DECREASE %	INCREASE %	DECREASE %
1	2						
F1	A1		9.3		27.8		41.0
F1	C1		8.7		22.2		4.2
F1	C2		8.2		23.1		8.0
F2	A1		6.9		27.2		38.5
F2	C1		6.4		21.5		0.0
F2	C2		5.9		22.5		4.0
AVERAGE			7.6		24.1		15.9

Table 11: Effect of Metal Deck Slabs with Transverse Ribs

EFFECT OF LATERAL SUPPORT AT THE COLUMN							
TESTS (WITH LATERAL SUPPORT)	TESTS (NO LATERAL SUPPORT)	MAXIMUM STRENGTH RATIO		INITIAL STIFFNESS		DUCTILITY FACTOR	
		INCREASE %	DECREASE %	INCREASE %	DECREASE %	INCREASE %	DECREASE %
1	2						
A1	B1	5.5		4.0		4.0	
A2	B2	1.8		1.6			12.5
AVERAGE		3.7		2.8			4.3

Table 12: EFFECT OF LATERAL SUPPORT AT THE COLUMN

TEST VARIABLE	MAXIMUM STRENGTH RATIO		INITIAL STIFFNESS		DUCTILITY FACTOR	
	INCREASE %	DECREASE %	INCREASE %	DECREASE %	INCREASE %	DECREASE %
SHRINKAGE GAP		1.0		29.5		18.5
INCREASED CONNECTOR DENSITY	0.3			4.1	9.8	
INCREASED CONCRETE STRENGTH	8.7		3.6			15.9
INCREASED BEAM DEPTH	3.1			11.2	4.5	
METAL DECK (LONGITUDINAL RIBS)		9.0		20.3		7.9
METAL DECK (TRANSVERSE RIBS)		7.6		24.1		15.9
LATERAL SUPPORT	3.7		2.8			4.3
REPEATED LOADS	0.0		0.0		0.0	

TABLE 13: SUMMARY OF TEST RESULTS

TEST NO	MAXIMUM STRENGTH RATIO $M/M_{MAX\ P}$			UPPER BOUND / TEST	TEST / LOWER BOUND
	TEST	UPPER BOUND	LOWER BOUND		
A1	1.73	2.03	1.53	1.17	1.13
A2	1.68	2.03	1.53	1.21	1.10
B1	1.64	2.13	1.54	1.30	1.07
B2	1.65	2.13	1.54	1.29	1.07
C1	1.72	2.22	1.61	1.29	1.07
C2	1.71	2.07	1.61	1.21	1.06
D1	1.75	2.22	1.61	1.27	1.09
D2	1.79	2.08	1.61	1.16	1.11
E1	1.59	1.81	1.48	1.14	1.07
E2	1.54	1.80	1.48	1.17	1.04
F1	1.57	1.80	1.48	1.15	1.06
F2	1.61	1.80	1.48	1.12	1.09
G1	1.87	2.18	1.72	1.16	1.09
G2	(1.65)	2.18	1.72	(1.32)	(0.96)
H1	1.68	1.91	1.67	1.14	1.01
H2	1.65	1.91	1.67	1.15	1.00

Table 14: CORRELATION OF THEORETICAL AND TEST VALUES OF MAXIMUM STRENGTH RATIO

TEST NO	INTERNAL DISSIPATION OF ENERGY (Kip in)								
	1	2	3	4	5	6	7	8	TOTAL
A1	377	0	1070	1710	232	147	35	365	3936
A2	377	0	1070	1710	232	147	35	365	3936
B1	351	300	1283	1710	159	147	257	0	4207
B2	351	300	1283	1710	159	147	257	0	4207
C1	453	0	1222	1710	172	147	290	383	4377
C2	465	0	1167	1710	188	147	0	383	4060
D1	451	0	1283	1710	159	147	257	384	4391
D2	472	0	1167	1710	188	147	0	384	4068
E1	464	0	1070	1710	67	45	24	131	3511
E2	464	0	1070	1710	67	45	4	131	3491
F1	466	0	1070	1710	67	45	10	131	3499
F2	466	0	1070	1710	67	45	4	131	3493
G1	637	0	1105	1685	188	147	13	399	4174
G2	637	0	1105	1685	188	147	13	399	4174
H1	456	0	2568	3099	301	147	19	372	6962
H2	456	0	2568	3099	301	147	19	372	6962

Column 1: DISSIPATION IN SLAB - SHEAR DEFORMATION
2: DISSIPATION IN SLAB - SHEARING OF SIDES
3: DISSIPATION IN BEAM WEB
4: DISSIPATION IN BEAM FLANGE
5: DISSIPATION IN TRANSVERSE REINFORCEMENT
6: DISSIPATION IN LONGITUDINAL REINFORCEMENT
7: DISSIPATION IN SHEAR CONNECTORS
8: DISSIPATION IN SLAB IN BENDING

Table 15: BREAK - DOWN OF THE INTERNAL DISSIPATION IN THE UPPER BOUND MECHANISM

TEST NO	TEST SET-UP (Span in inches)	W (in)	T (in)	BEAM SIZE	$\frac{M_{max}}{M_{Lower\ Bound}}$ 0 0.5 1.0	REF.
B-44	96	48	4 Solid	W12x27		1
B-64	144	72	4 "	W12x27		1
B-84	192	96	4 "	W12x27		1
B-66	144	72	6 "	W12x27		1
A1	97	48	4 "	W12x27		
A2	97	48	4 "	W12x27		
B1	97	48	4 "	W12x27		
B2	97	48	4 "	W12x27		
C1	97	48	4 "	W12x27		
C2	97	48	4 "	W12x27		
D1	97	48	4 "	W12x27		
D2	97	48	4 "	W12x27		
E1	97	48	4 Rib	W12x27		
E2	97	48	4 "	W12x27		
F1	97	48	4 "	W12x27		
F2	97	48	4 "	W12x27		
G1	97	48	4 Solid	W12x27		
G2	97	48	4 "	W12x27		
H1	97	48	4 "	W16x40		
H2	97	48	4 "	W16x40		

W = SLAB WIDTH

T = SLAB THICKNESS

Table 16: Summary of all tests to date

TEST NO	ROTATION CAPACITY (Radians)
A1	.042
A2	.040
B1	.042
B2	.034
C1	.028
C2	.037
D1	.050
D2	.048
E1	.027
E2	.040
F1	.022
F2	.022
G1	.037
G2	(.000)
H1	.038
H2	.050

Table 17: Rotation Capacity of each test

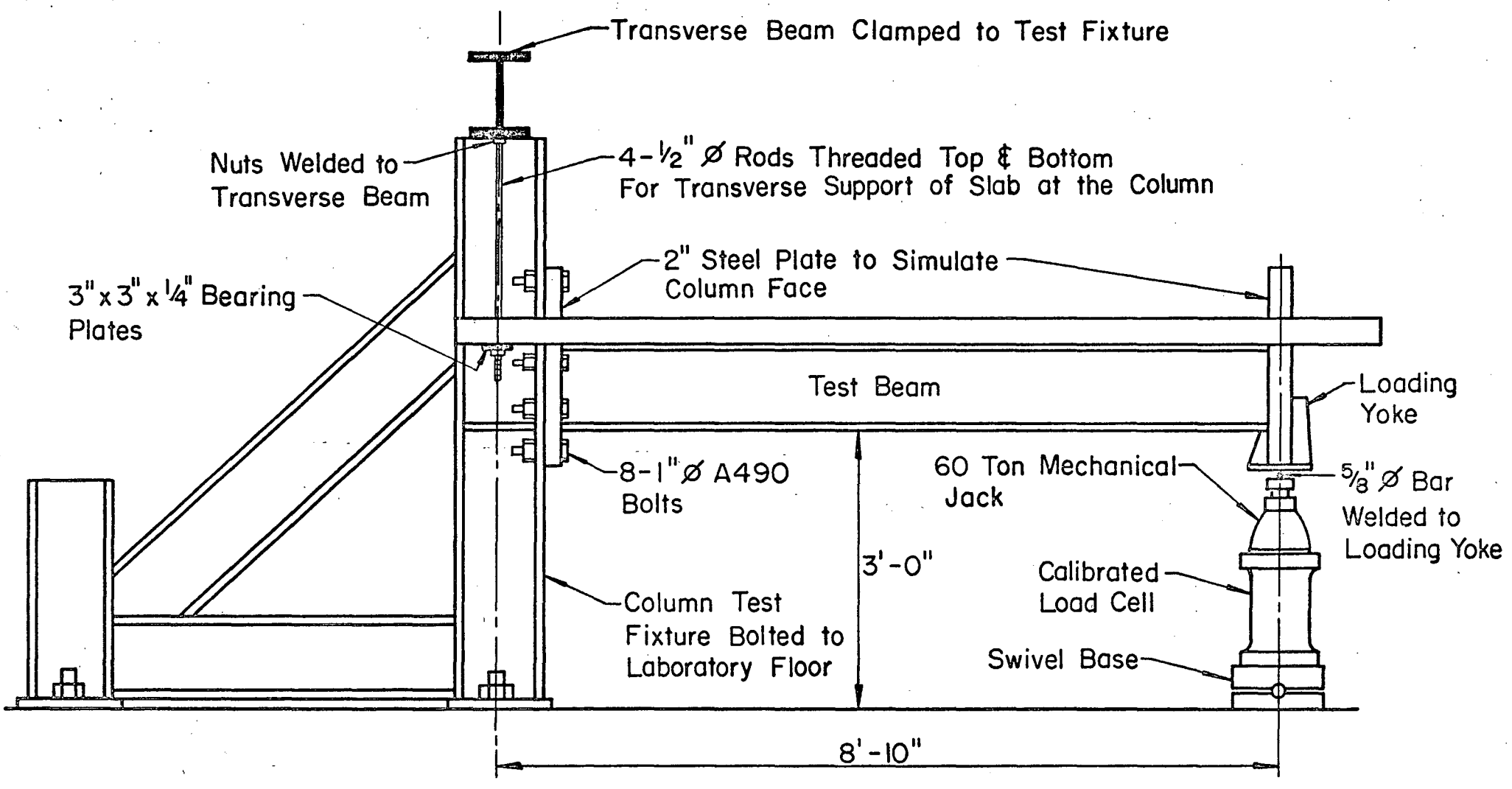

FIG. 1: SCHEMATIC VIEW OF TEST SET-UP

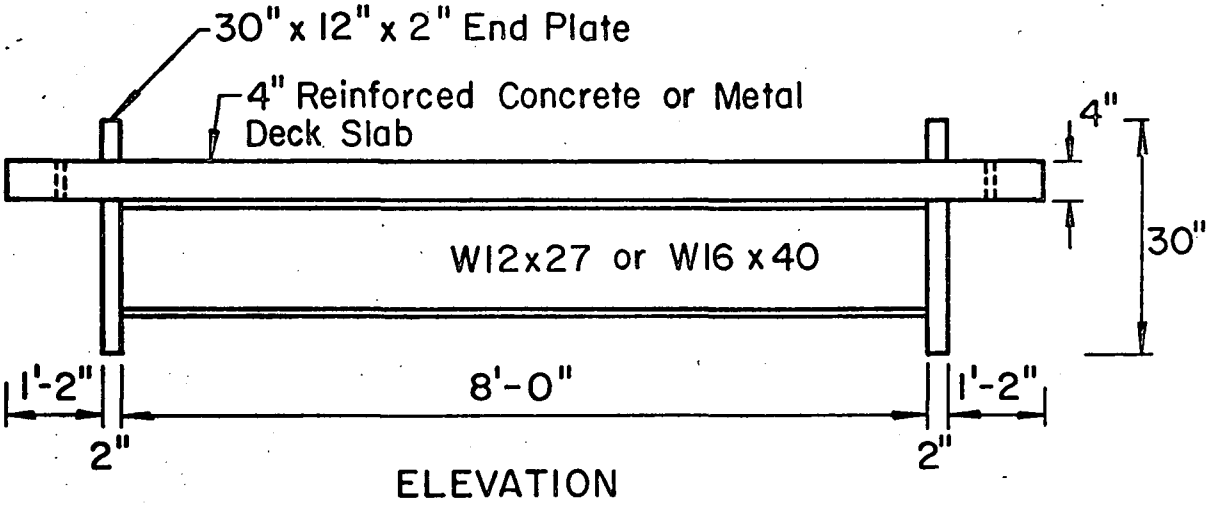

ELEVATION

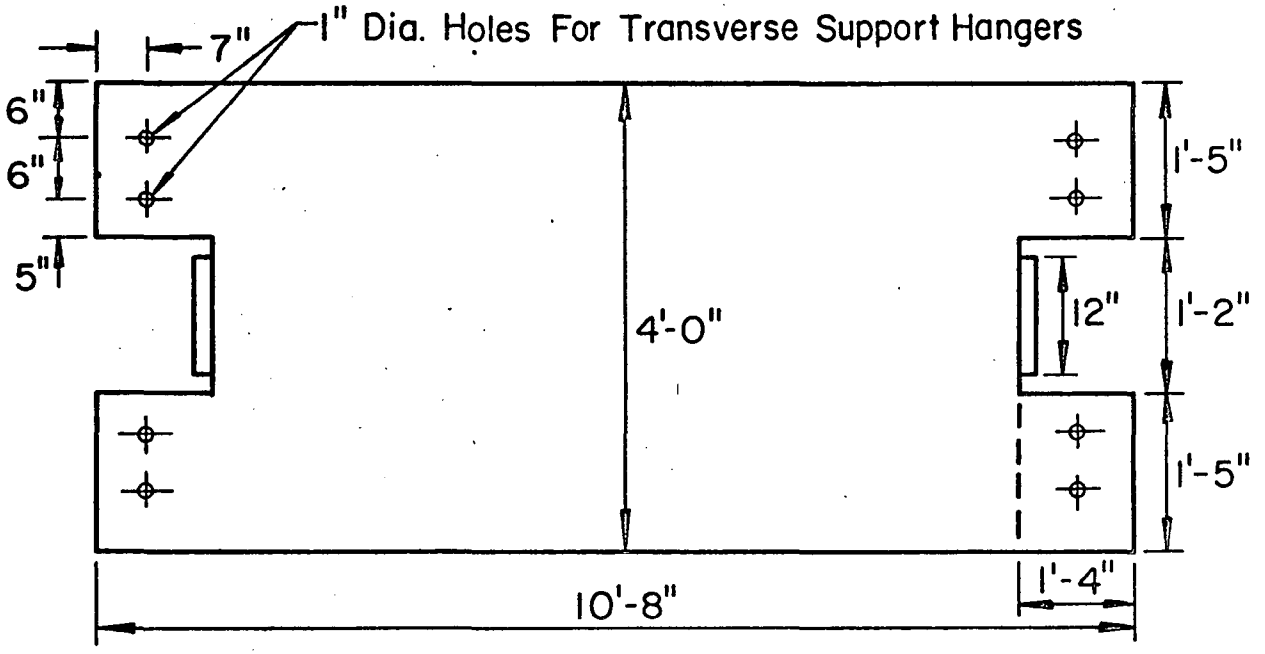

PLAN

FIG. 2: TYPICAL TEST BEAM

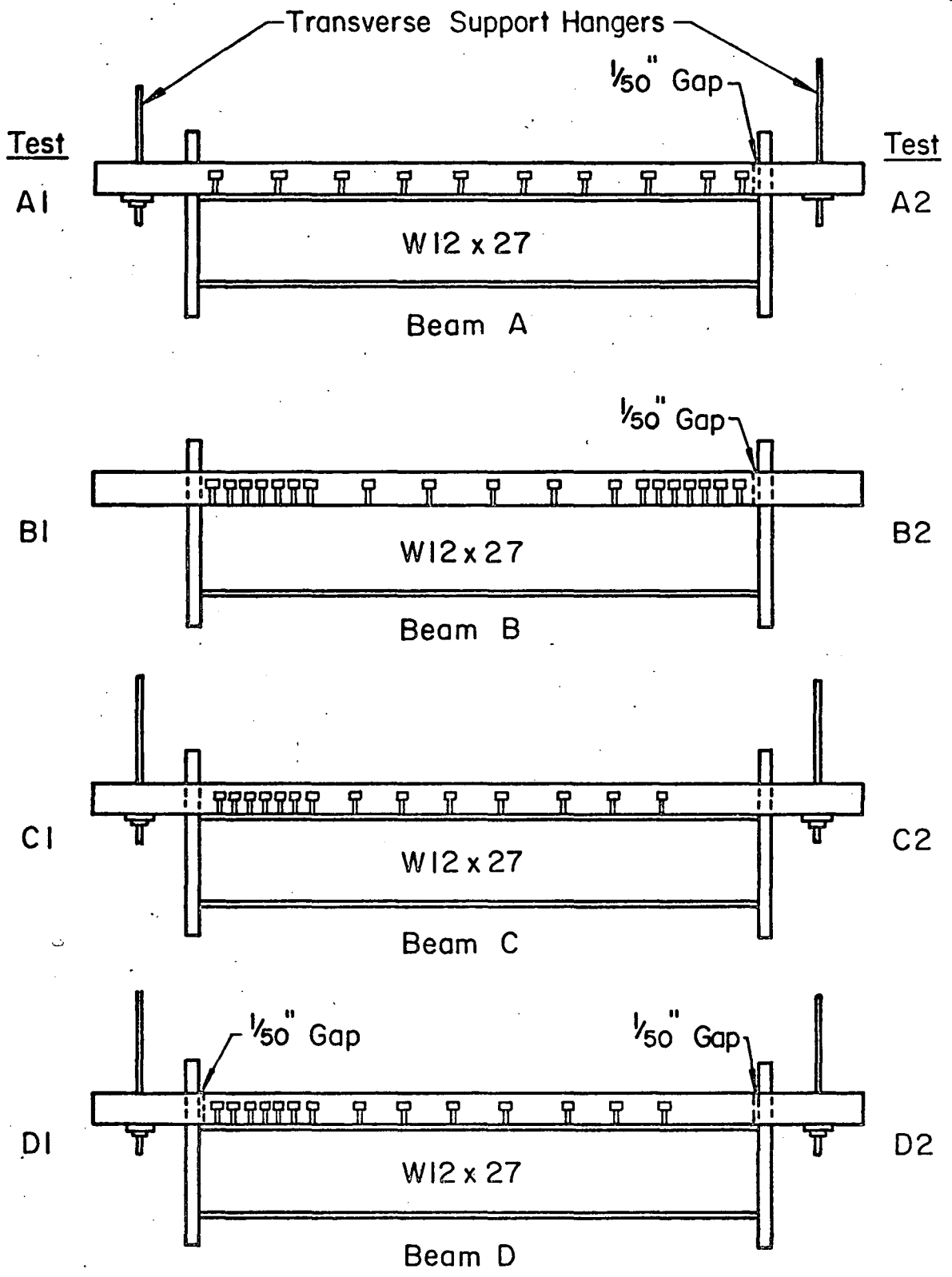

FIG. 3: DETAIL OF TEST BEAMS A, B, C & D

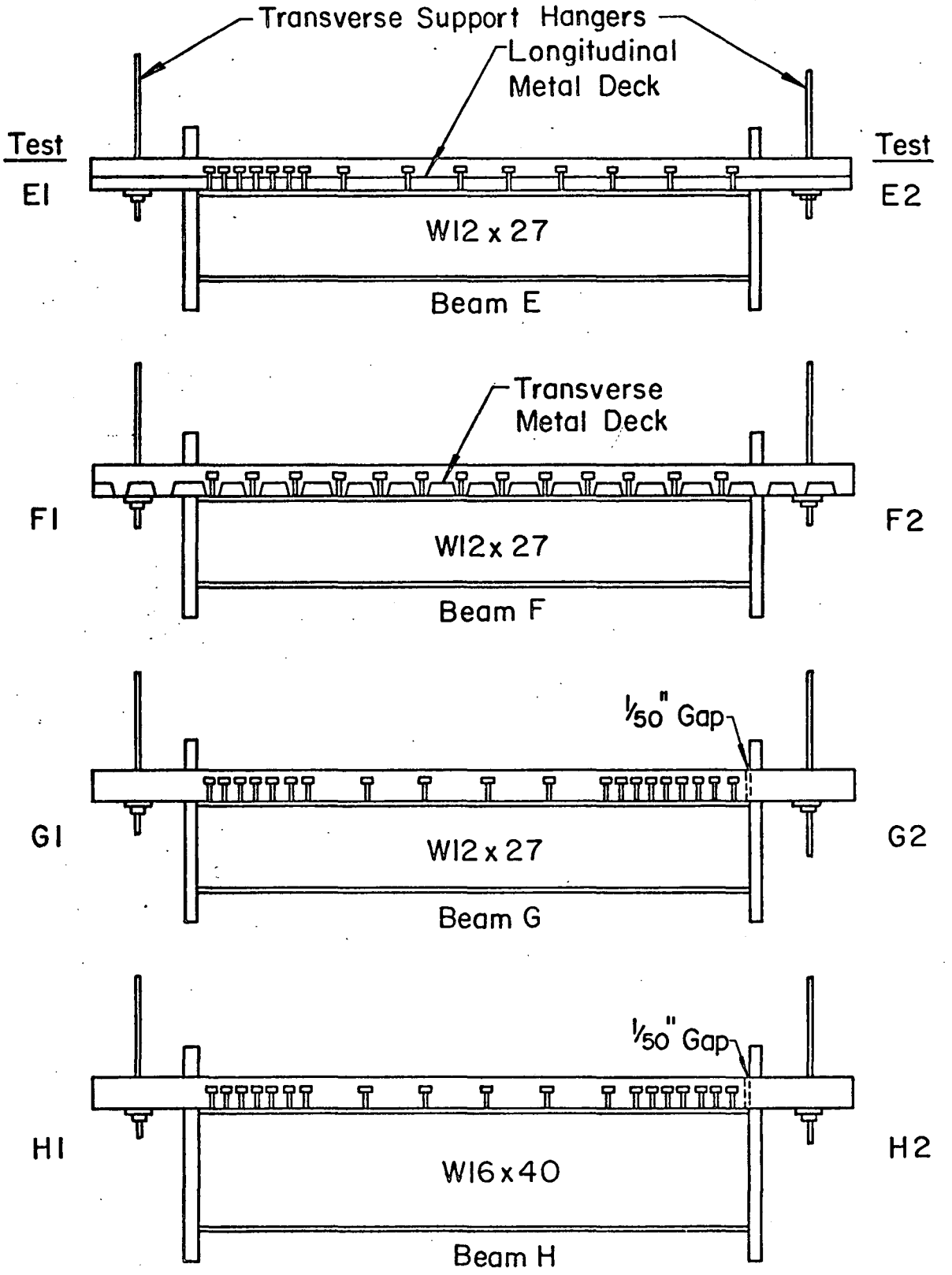

FIG. 4: DETAIL OF TEST BEAMS E, F, G & H

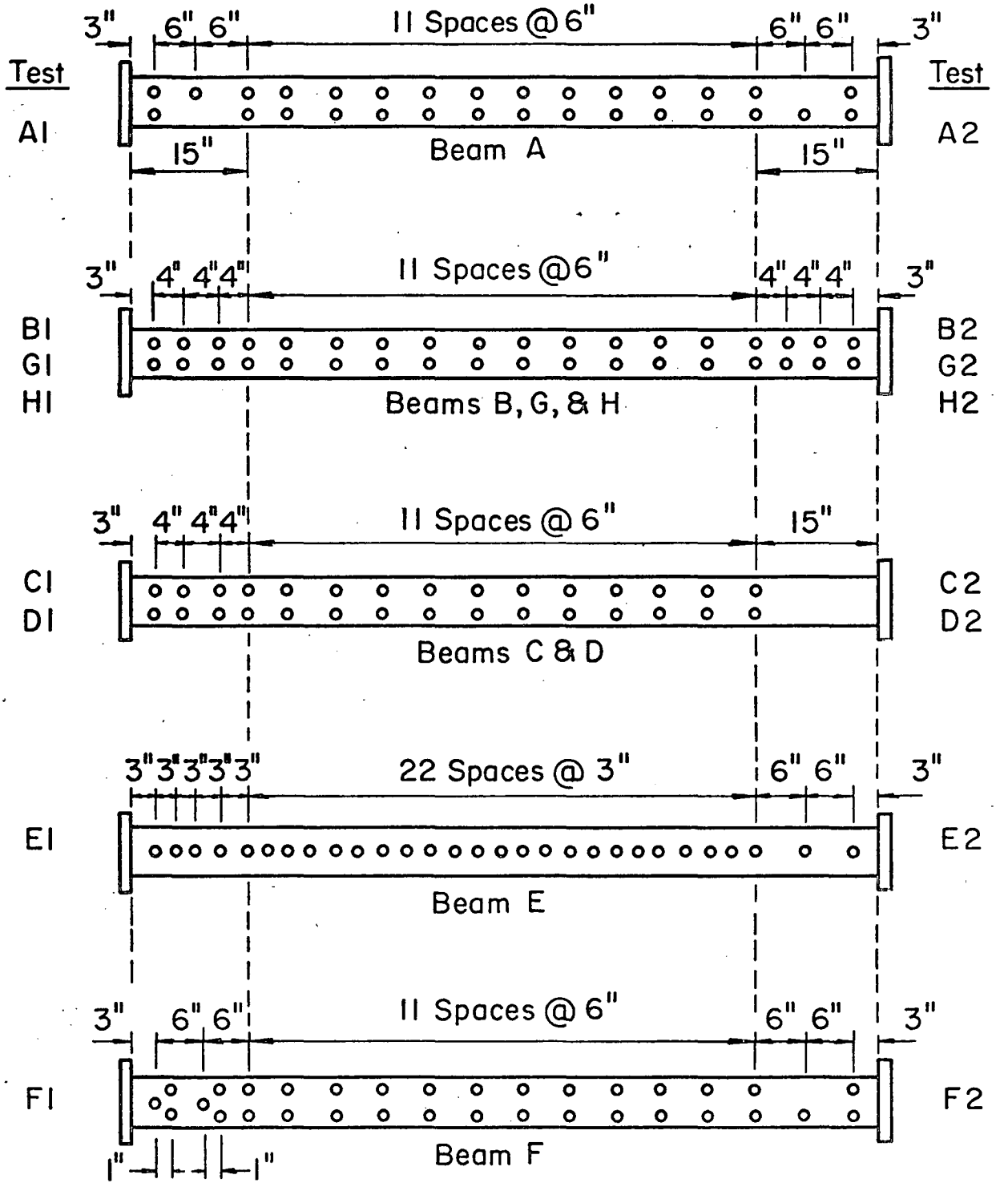

FIG. 5: DETAILS OF CONNECTOR SPACING

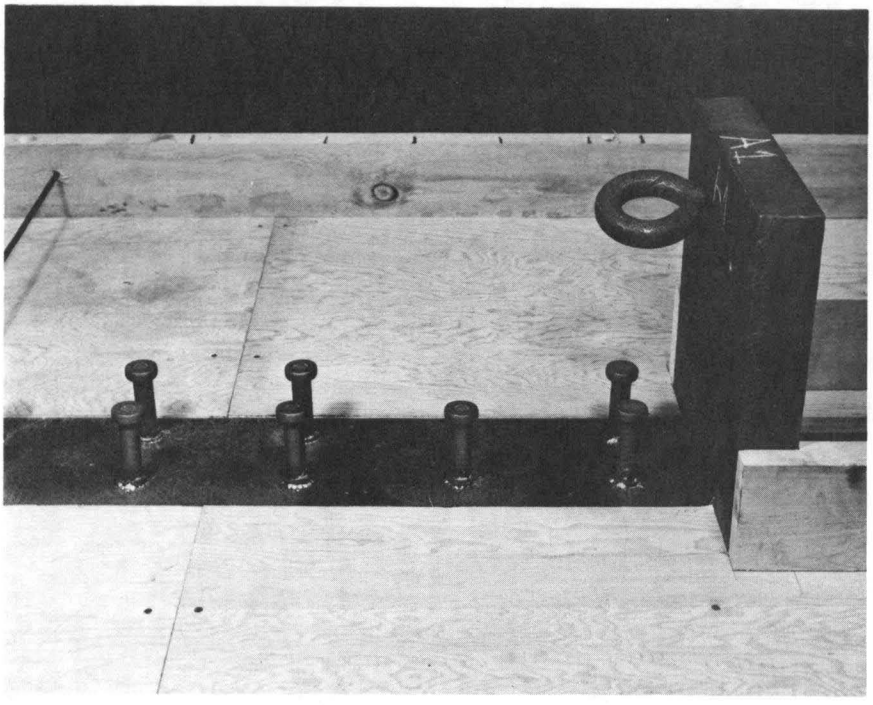

FIG.6a: TYPICAL NORMAL DENSITY CONNECTOR SPACING

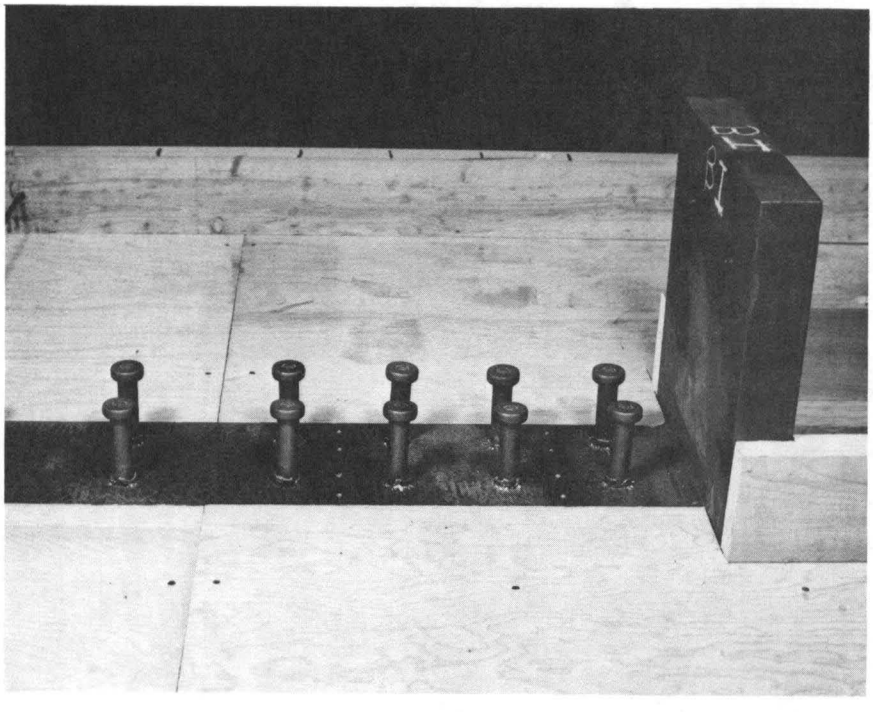

FIG.6b: TYPICAL HIGH DENSITY CONNECTOR SPACING

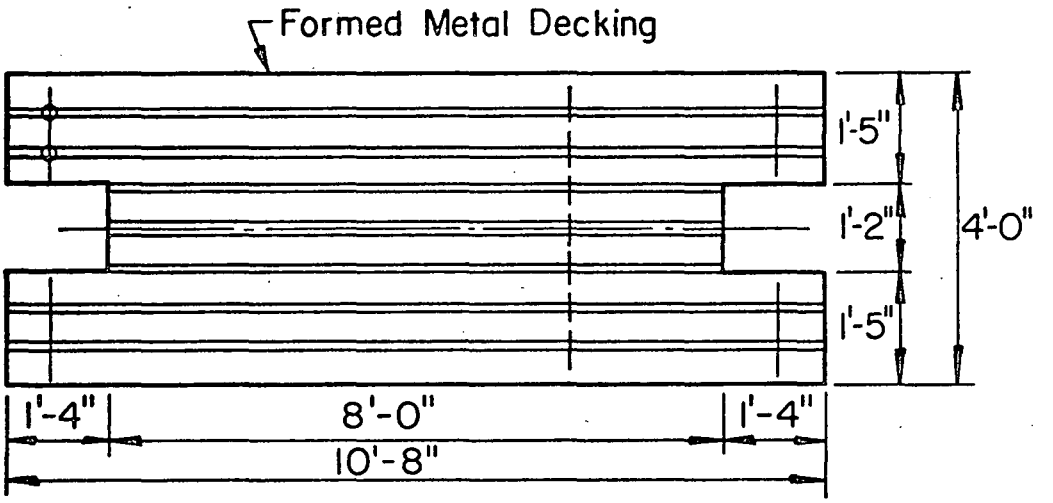

FIG. 7a: RIBS IN LONGITUDINAL DIRECTION (BEAM E)

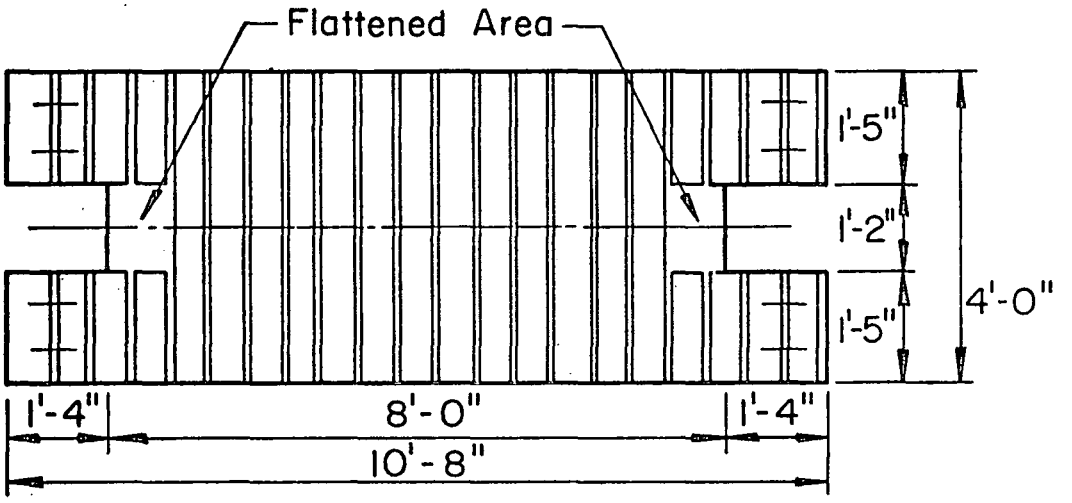

FIG. 7b: RIBS IN TRANSVERSE DIRECTION (BEAM F)

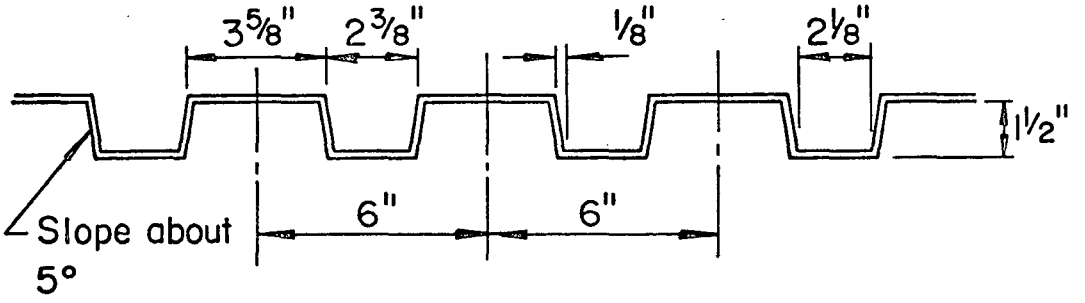

FIG. 7c: DETAIL OF METAL DECKING (GAGE 20)

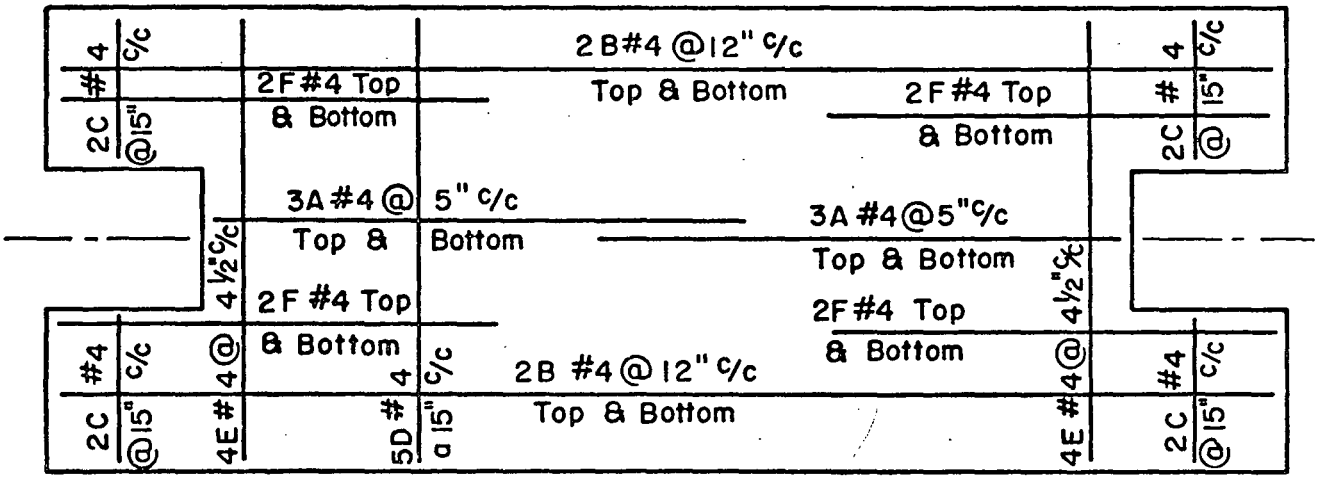

FIG. 8a: REINFORCEMENT DETAILS FOR BEAMS A, B, C, D, G & H

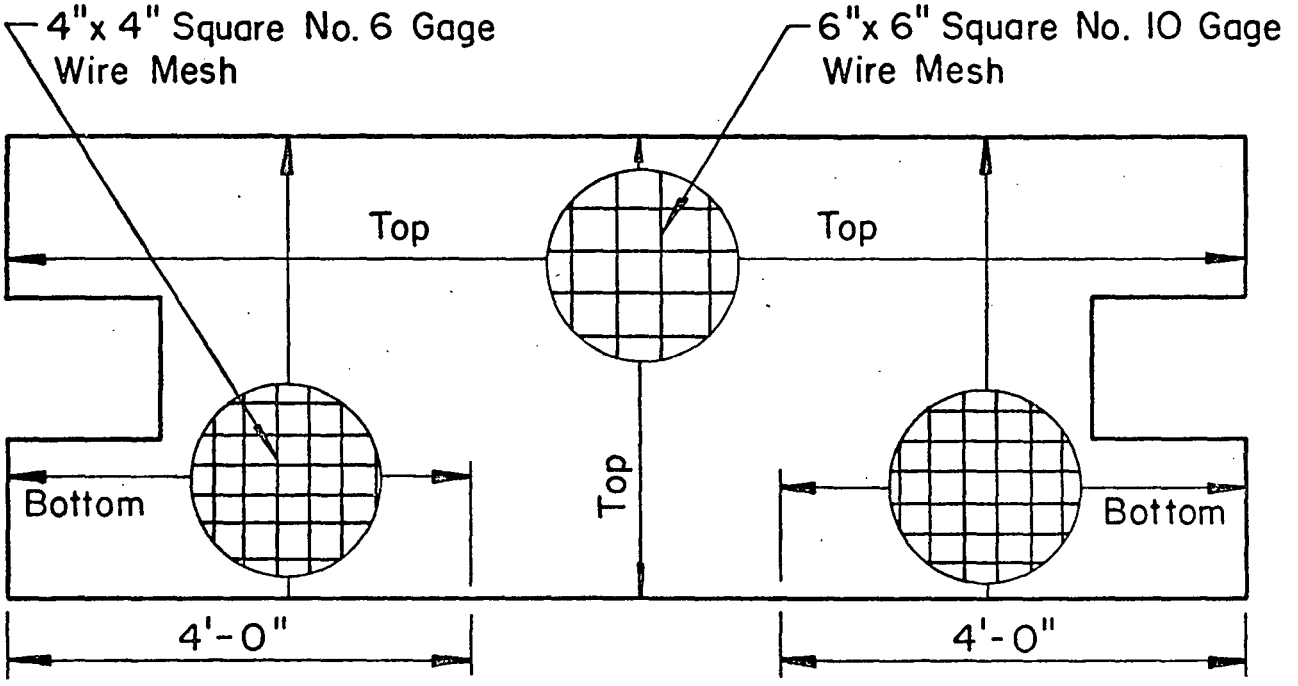

FIG. 8b: REINFORCEMENT DETAILS FOR BEAMS E & F

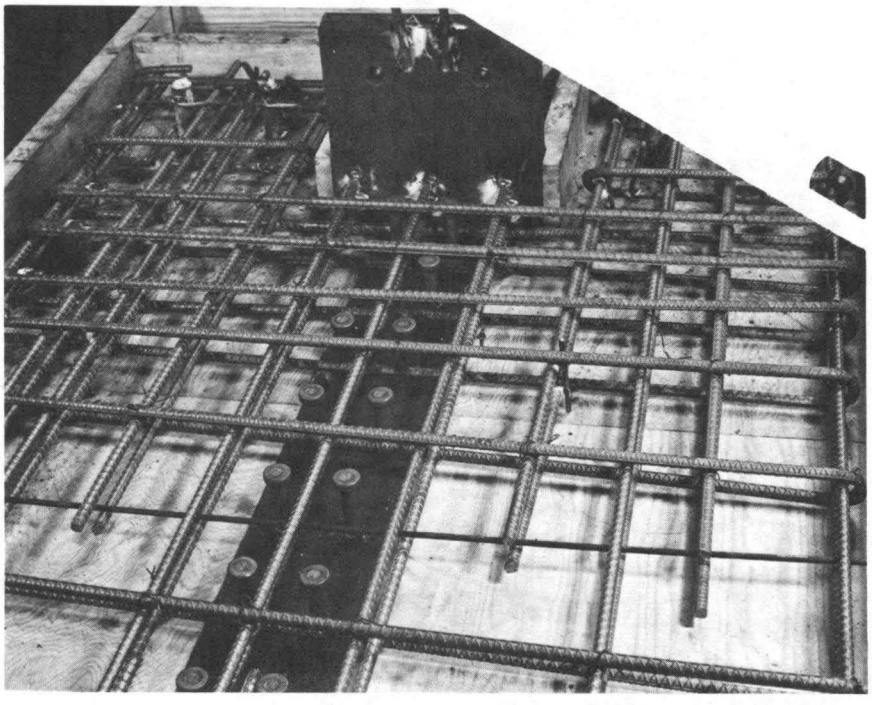

FIG.9a: REINFORCEMENT DETAIL FOR BEAM WITH NO SHRINAGE GAP

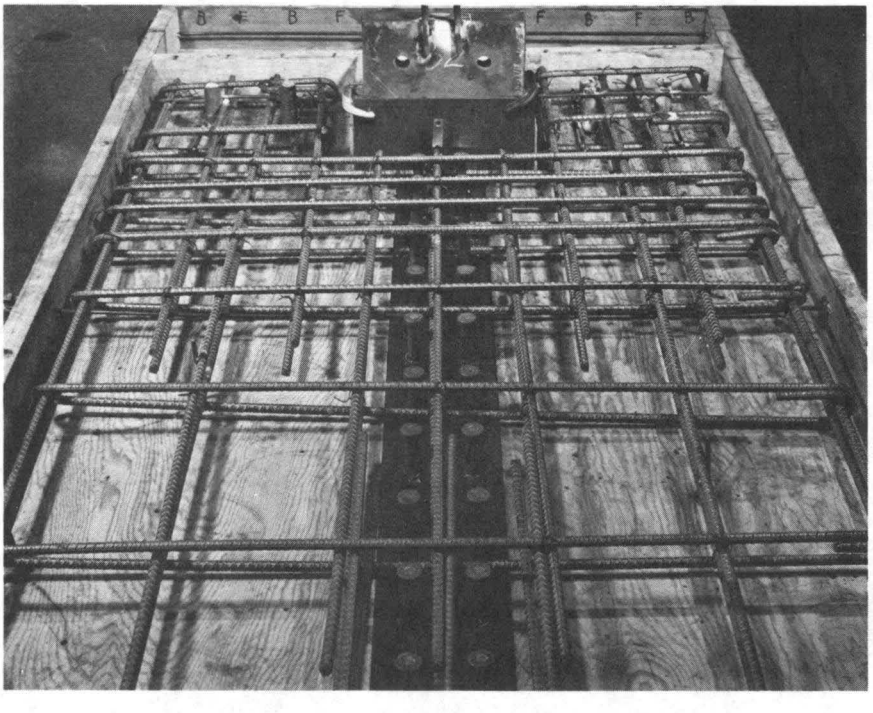

FIG.9b: REINFORCEMENT DETAIL FOR BEAM WITH SHRINKAGE GAP

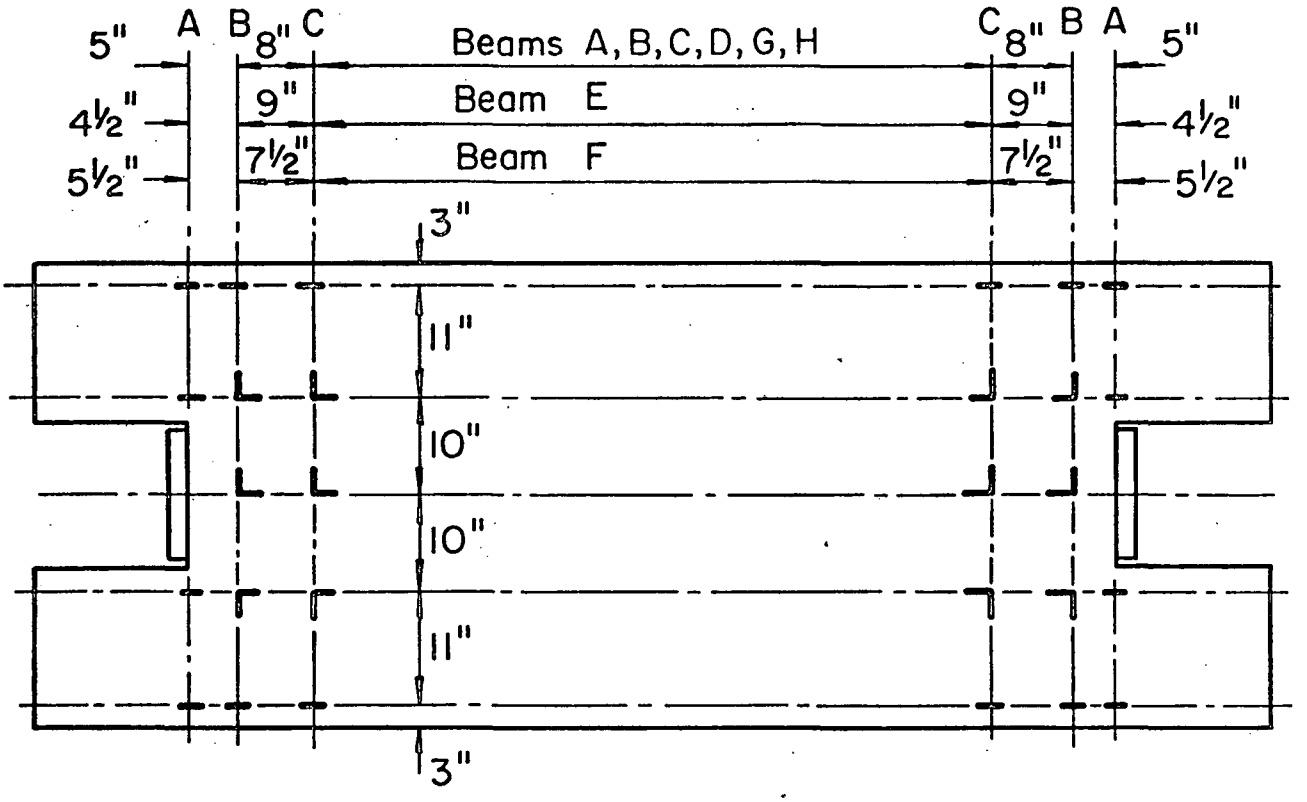

FIG. 10a: LOCATION OF ELECTRICAL RESISTANCE STRAIN GAGES ON CONCRETE SLAB

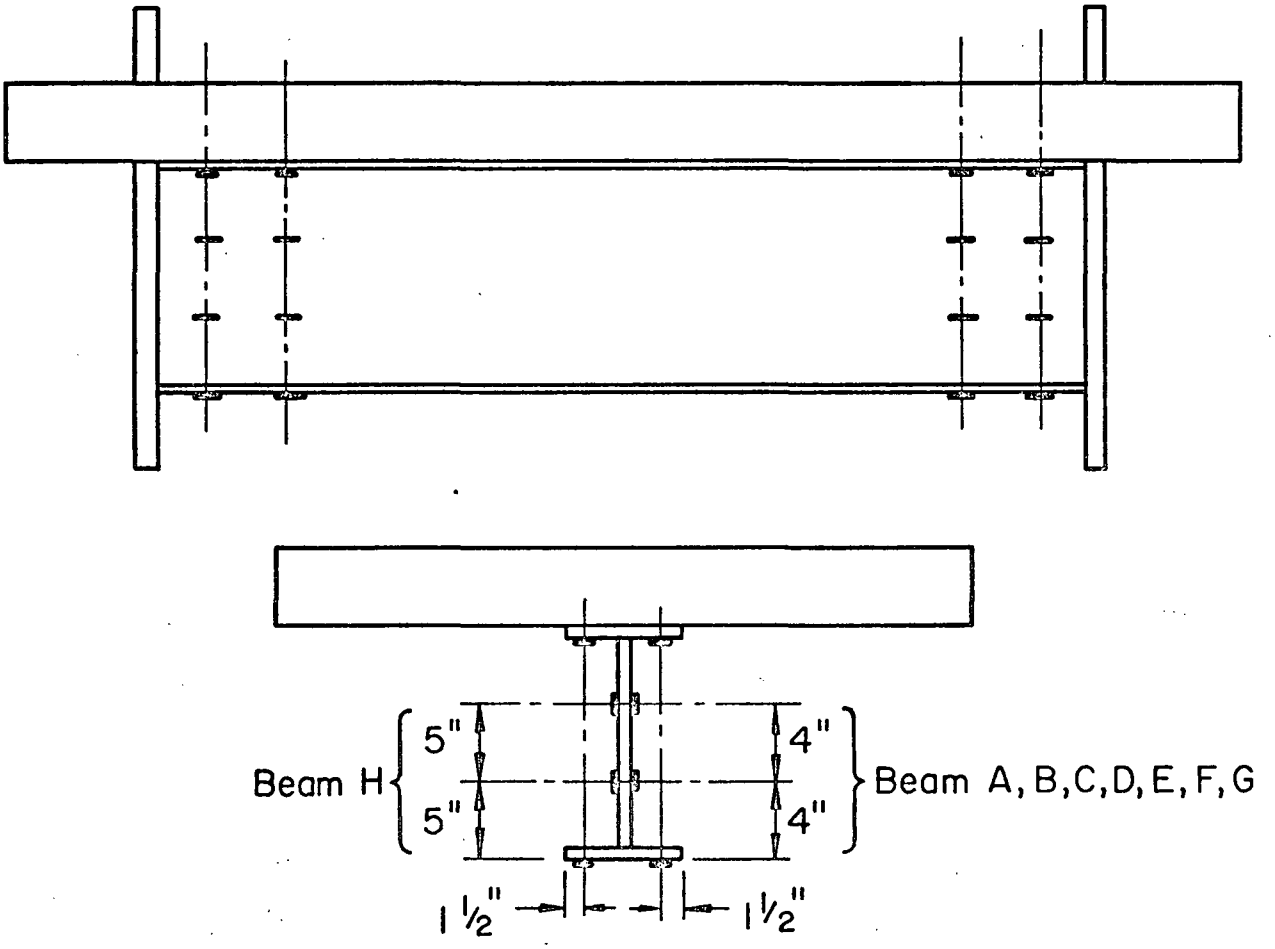

FIG. 10b: STRAIN GAGES ON STEEL BEAM

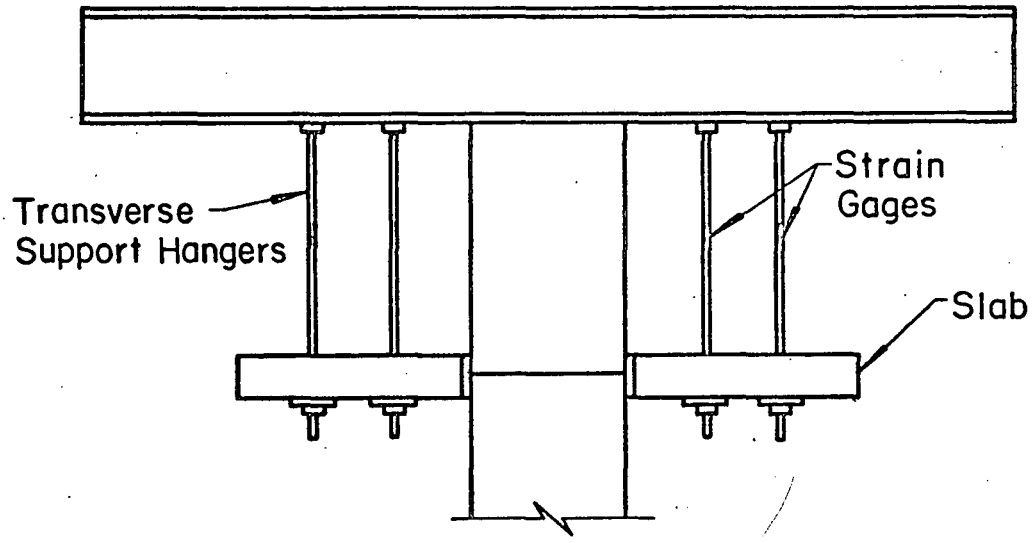

FIG. 11a: STRAIN GAGES ON TRANSVERSE SUPPORT HANGERS

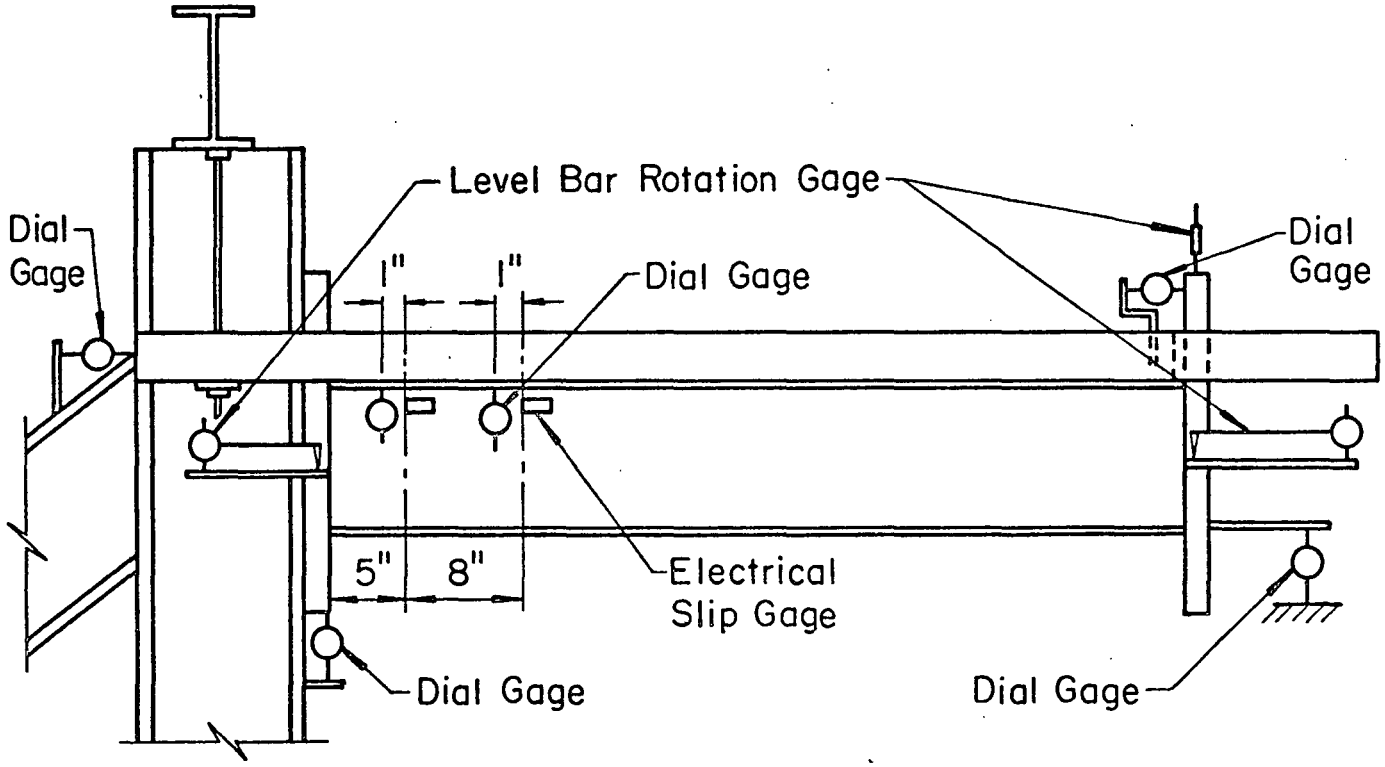

FIG. 11b: LOCATION OF AMES DIAL GAGES, ELECTRICAL SLIP GAGES AND ROTATION GAGES

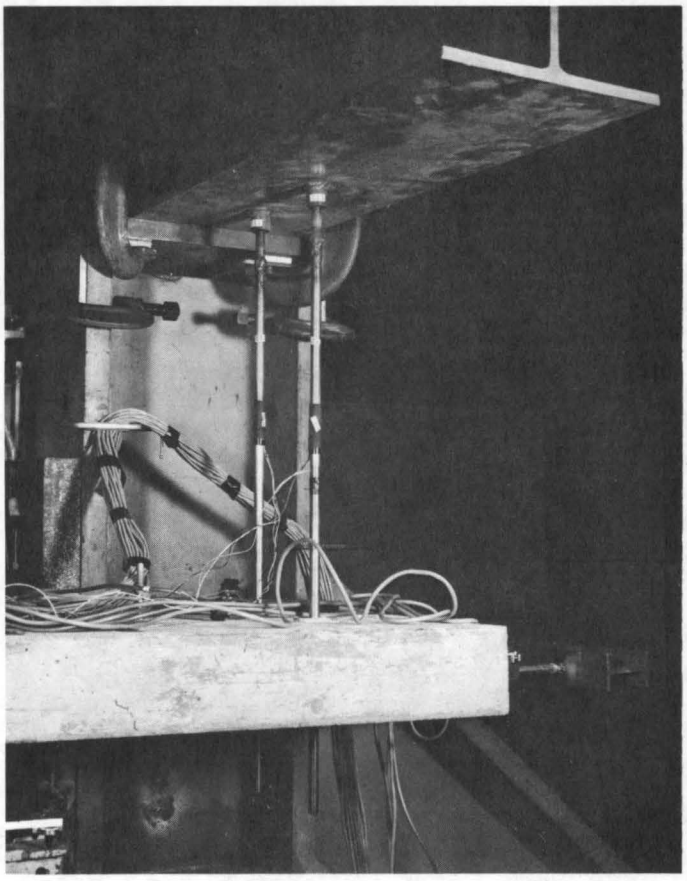

FIG.12a

DETAIL OF TRANSVERSE SUPPORT HANGERS AT TEST LOCATION

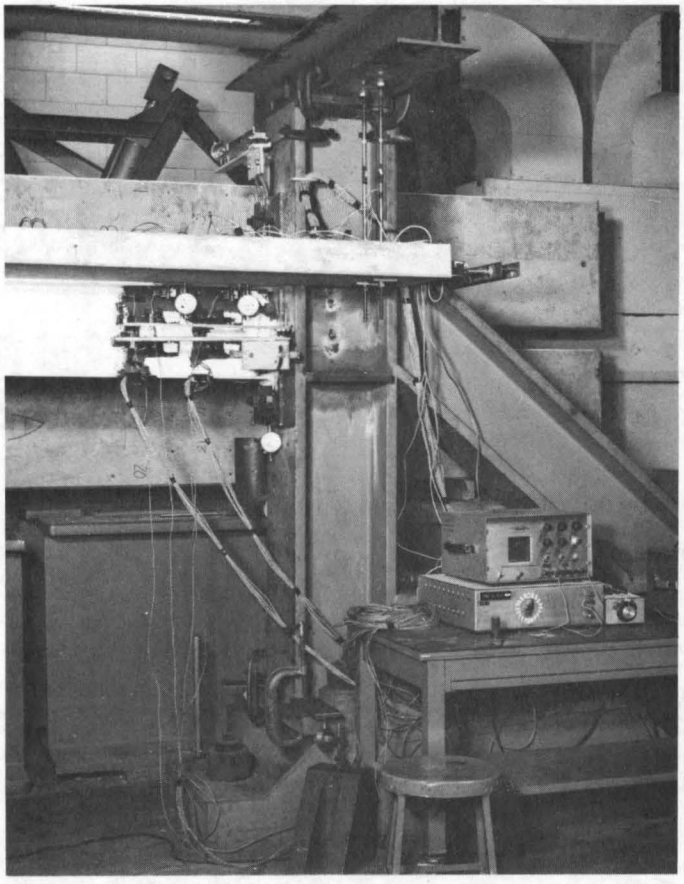

FIG.12b

INSTRUMENTATION AT THE TEST LOCATION

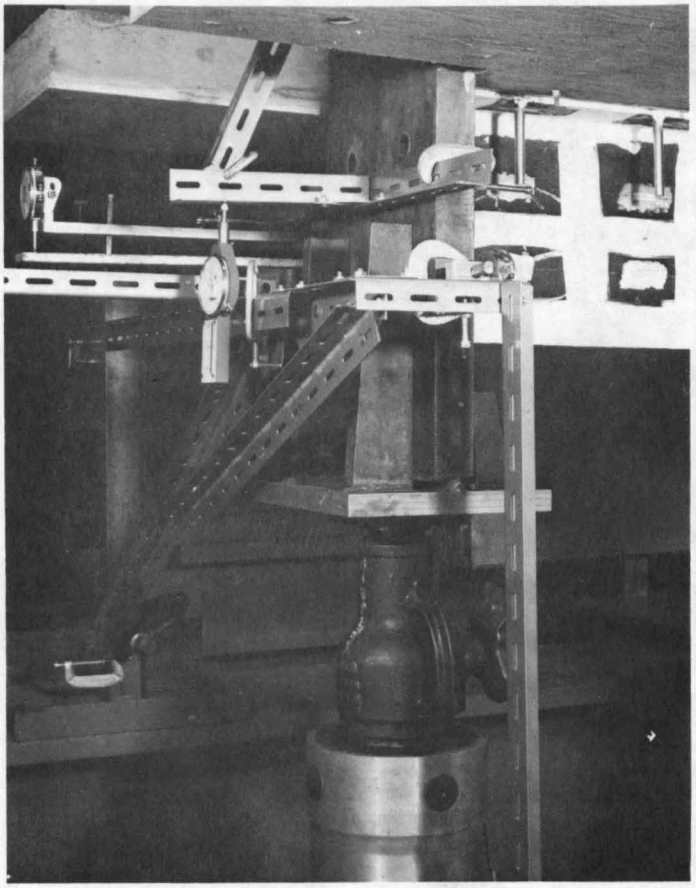

FIG.13a

INSTRUMENTATION AT THE LOAD POSITION

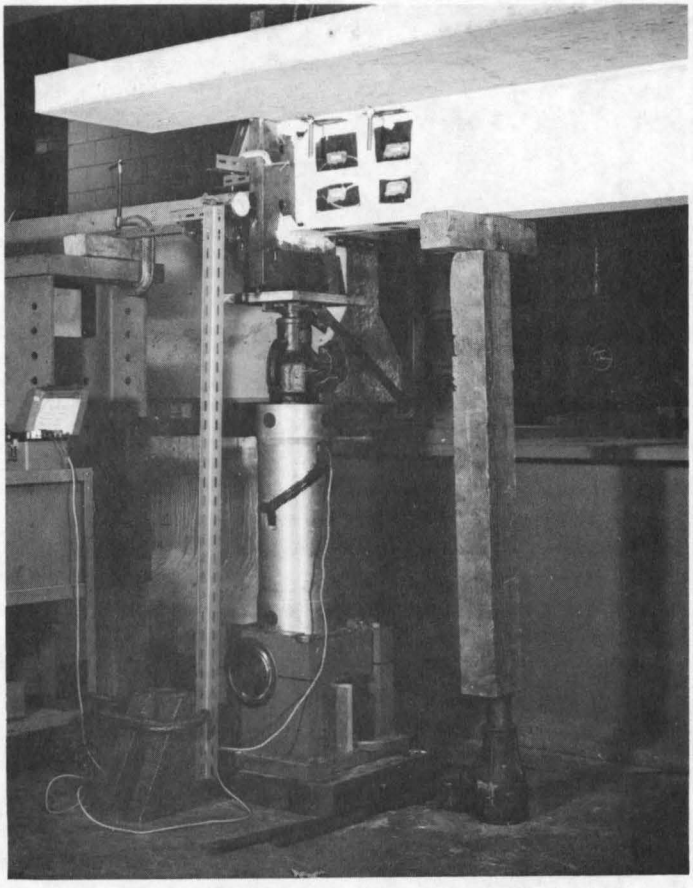

FIG.13b

METHOD OF LOADING

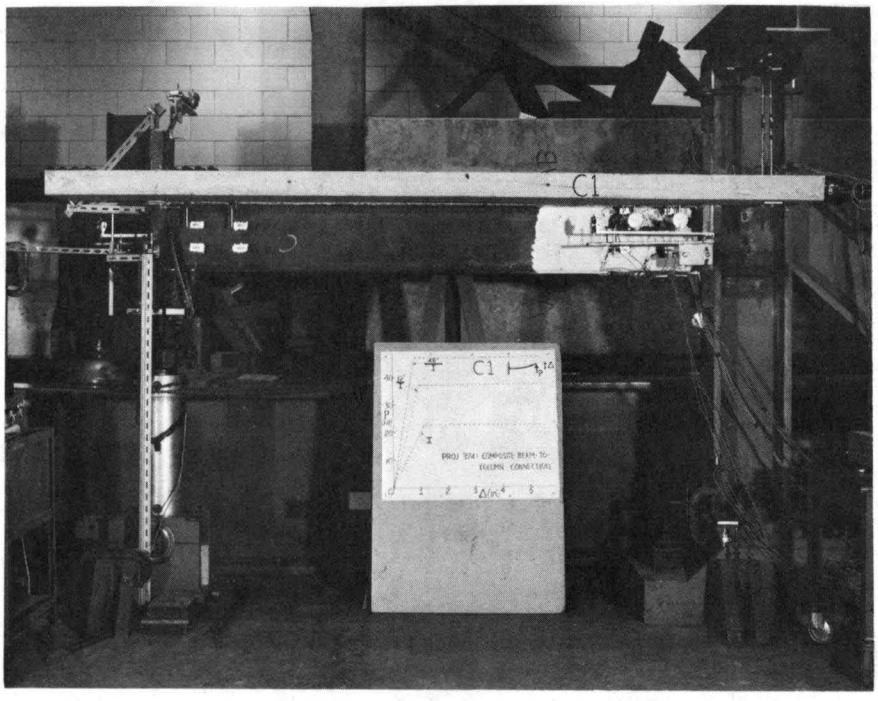

FIG.14a: VIEW OF BEAM C BEFORE TEST C1

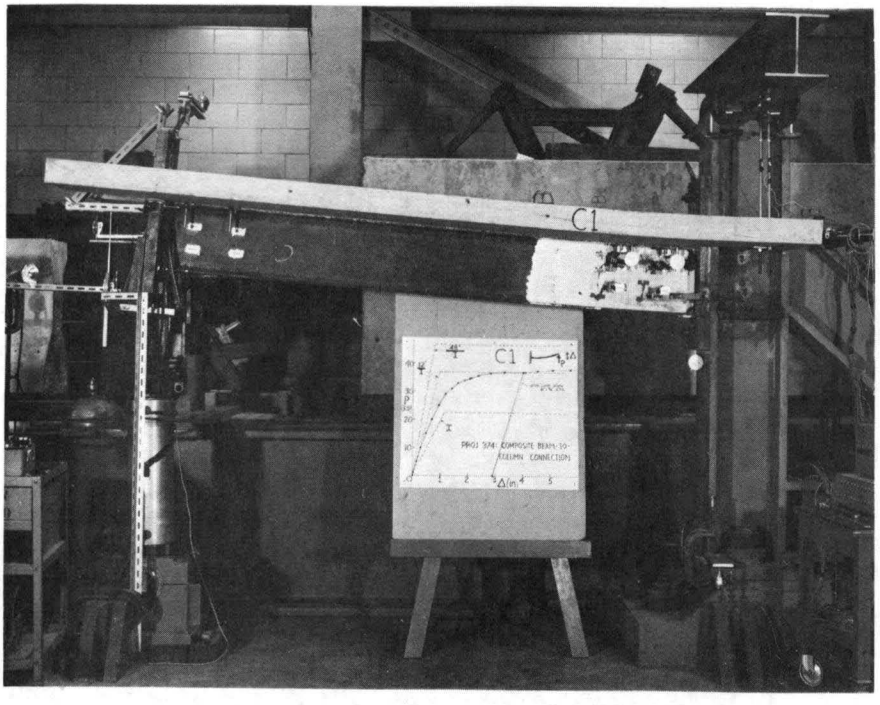

FIG.14b: VIEW OF BEAM C AFTER TEST C1

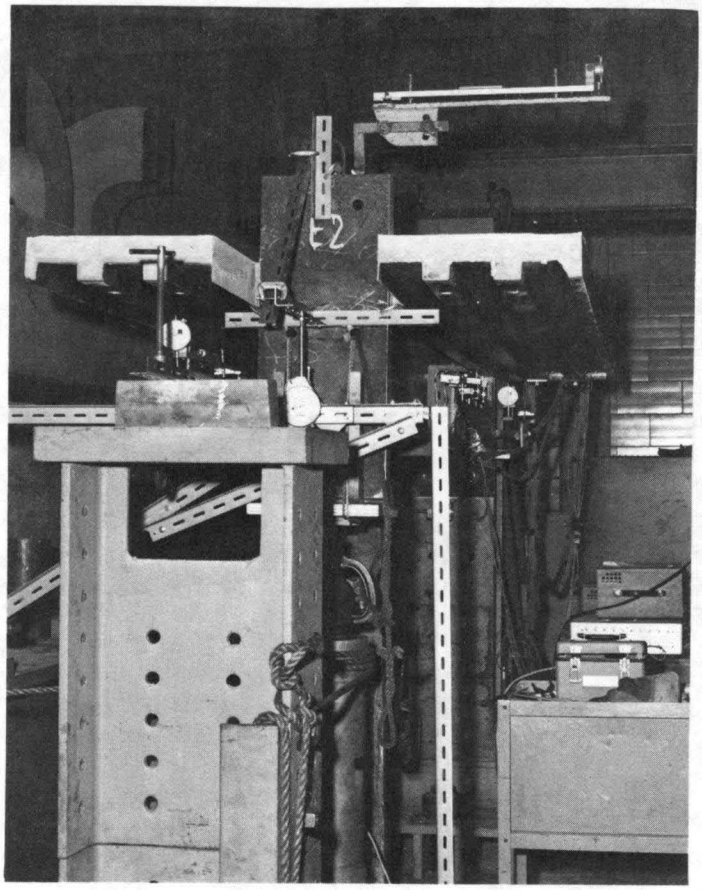

FIG.15a

BEAM E IN POSITION FOR TEST E1

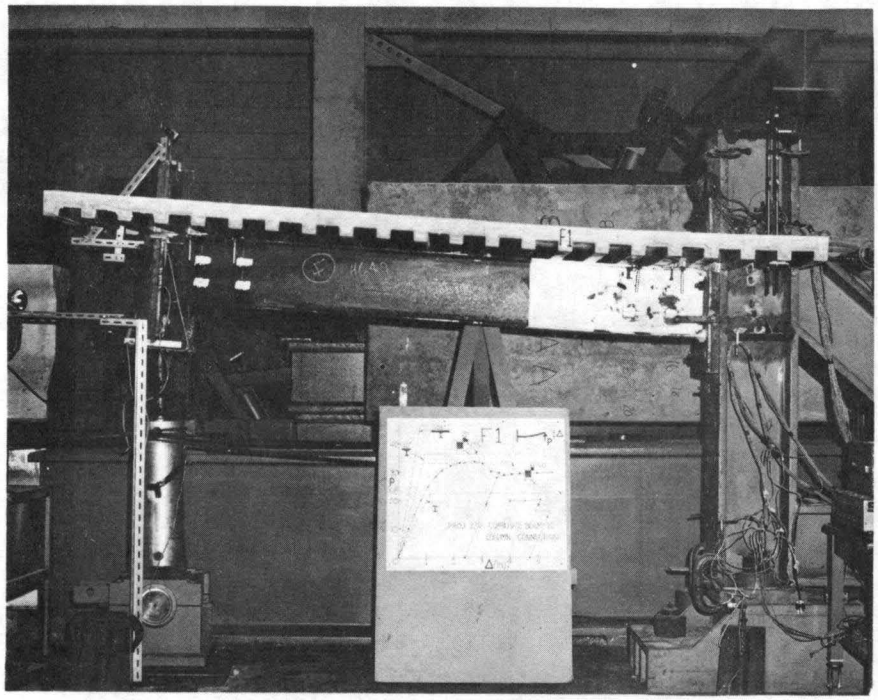

FIG.15b: BEAM F AT END OF TEST F1

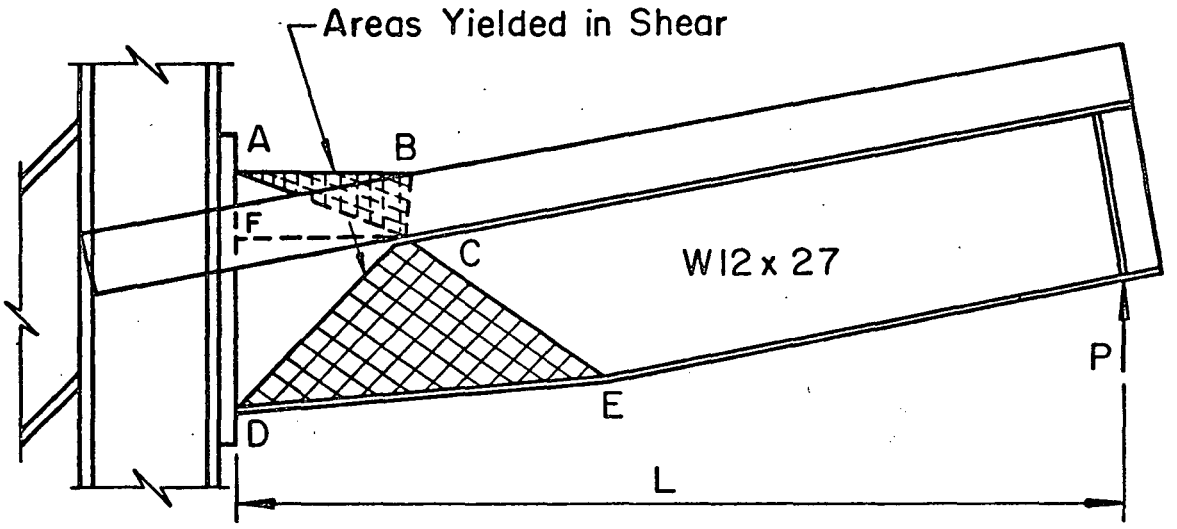

FIG. 16a: ASSUMED FAILURE MECHANISM FOR CONNECTIONS WITHOUT TRANSVERSE SUPPORT

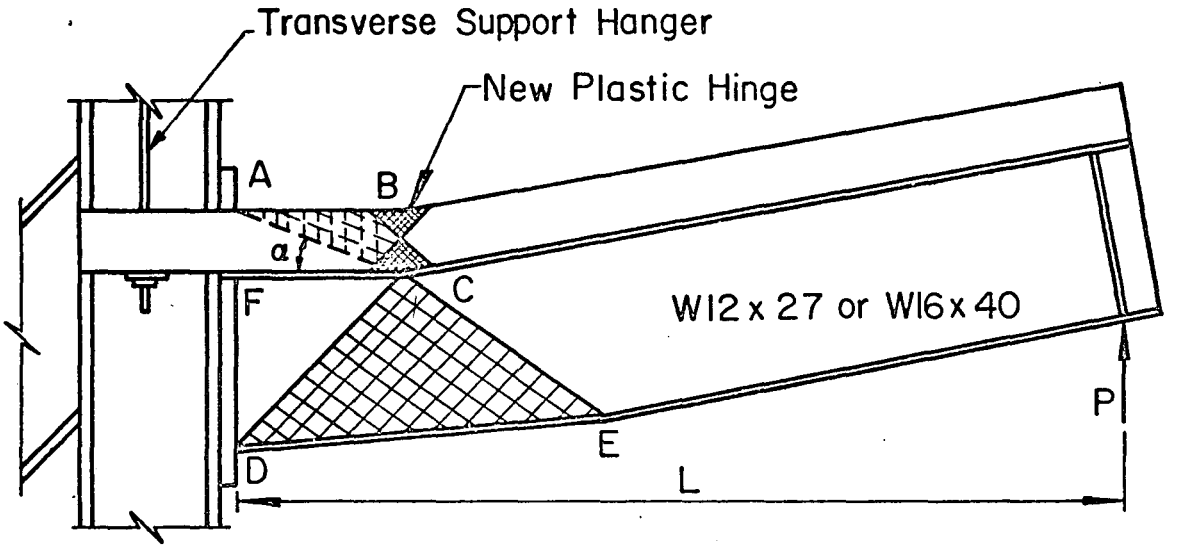

FIG. 16b: ASSUMED FAILURE MECHANISM FOR CONNECTIONS WITH TRANSVERSE SUPPORT

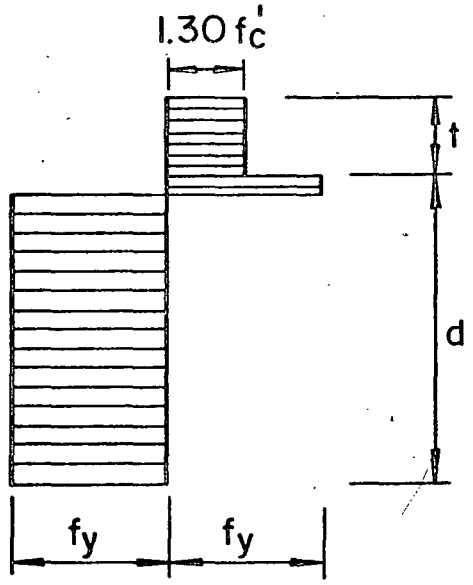

FIG. 17a: LOWER BOUND STRESS FIELD FOR CONNECTIONS WITHOUT TRANSVERSE SUPPORT

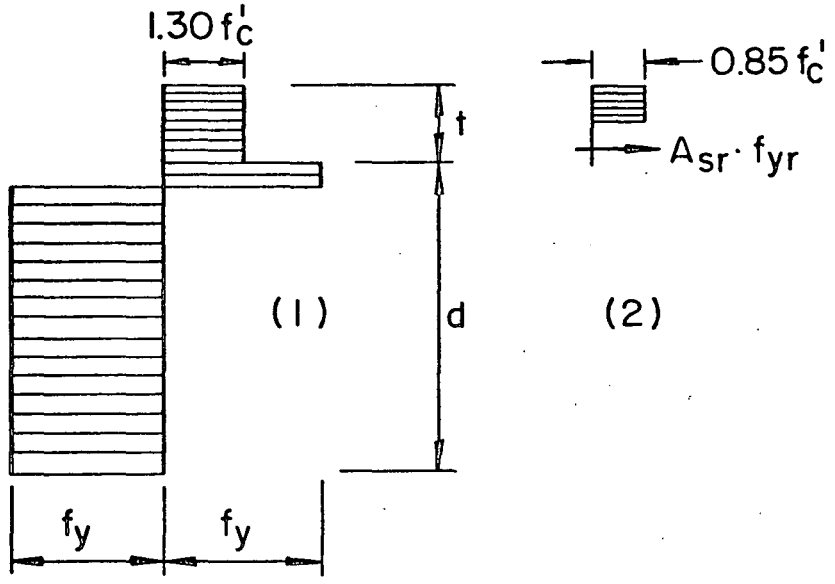

FIG. 17b: LOWER BOUND STRESS FIELD FOR CONNECTIONS WITH TRANSVERSE SUPPORT

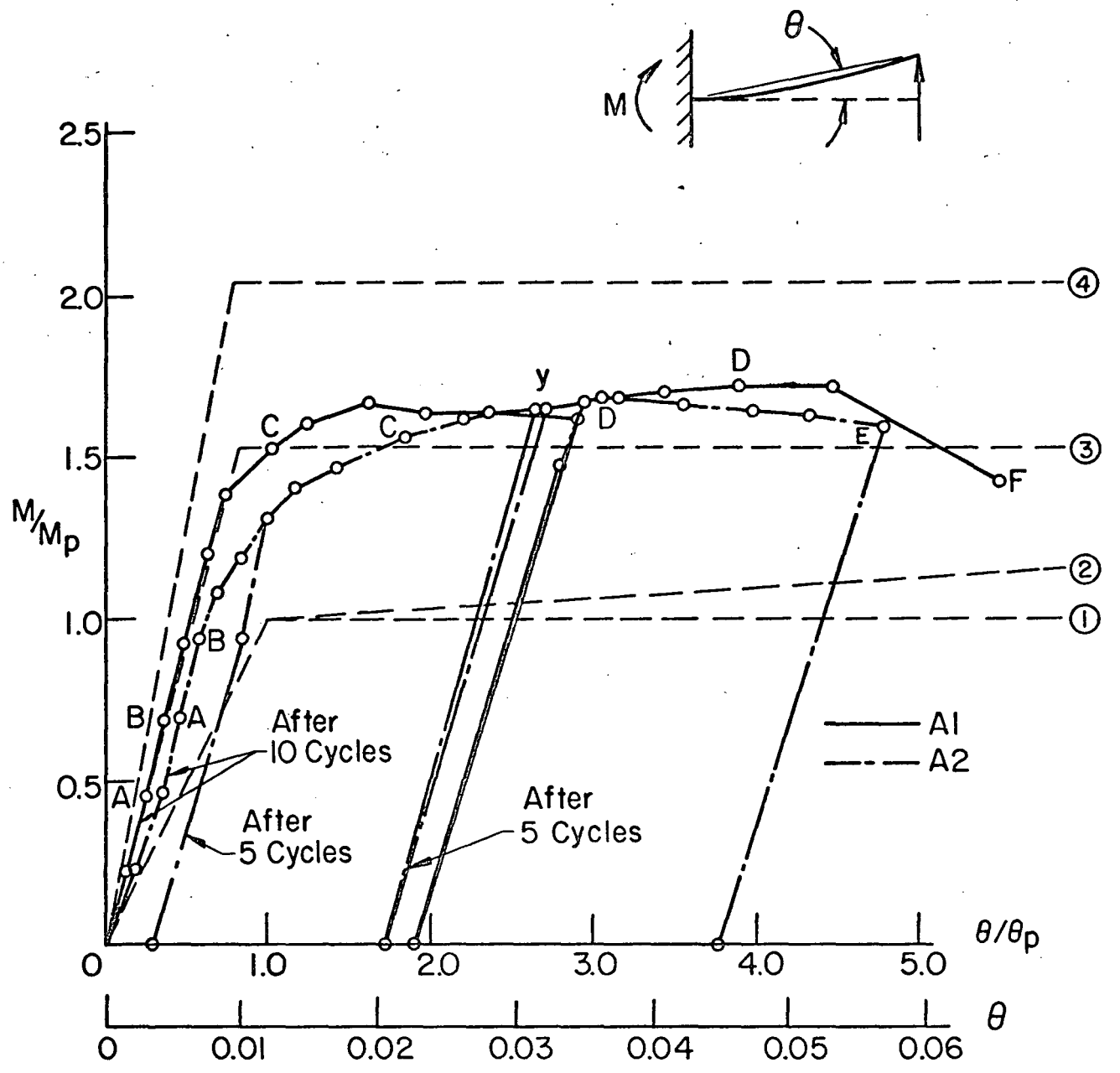

FIG. 18: MOMENT - ROTATION BEHAVIOR : TESTS A1 & A2

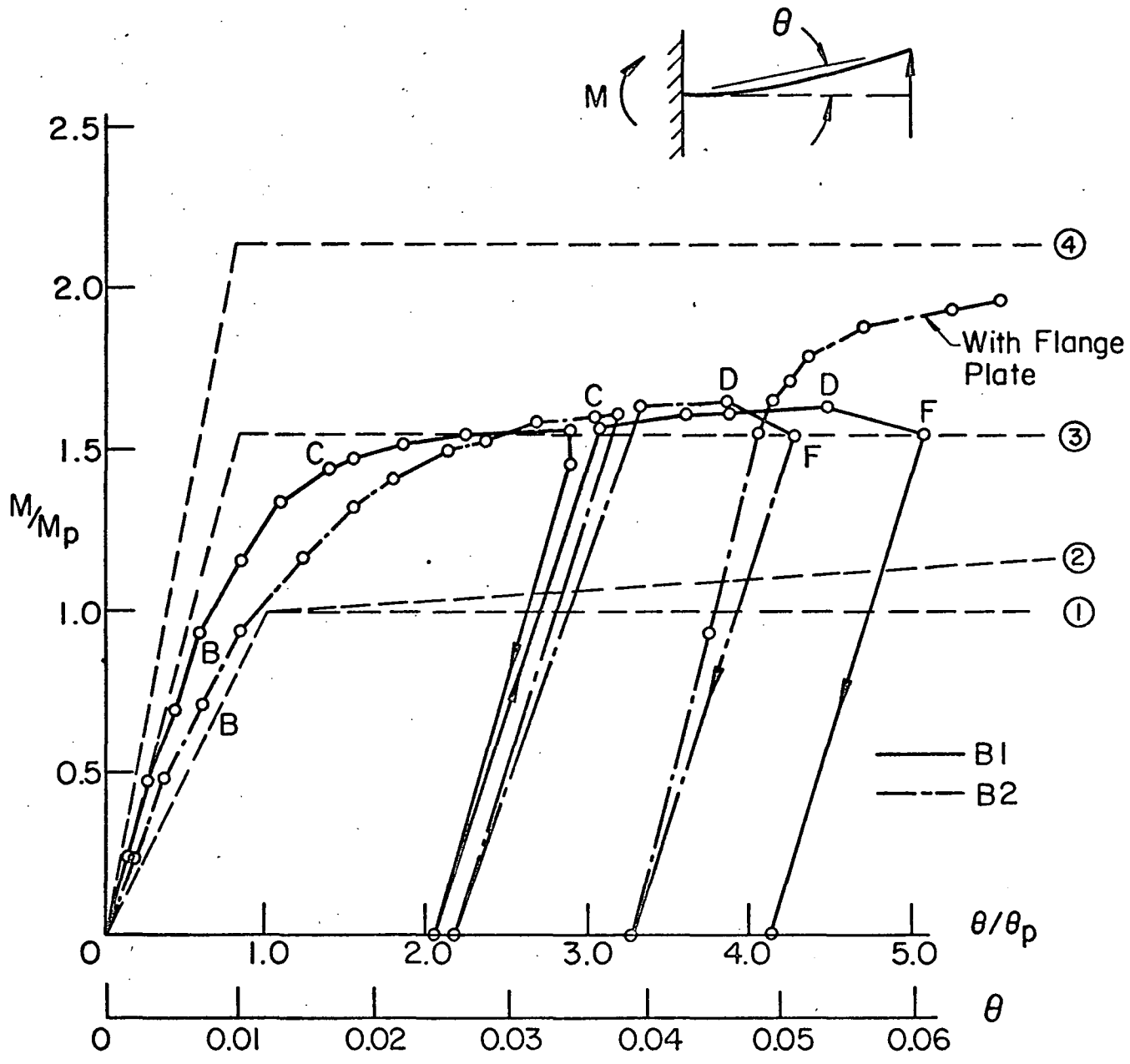

FIG. 19: MOMENT - ROTATION BEHAVIOR : TESTS B1 & B2

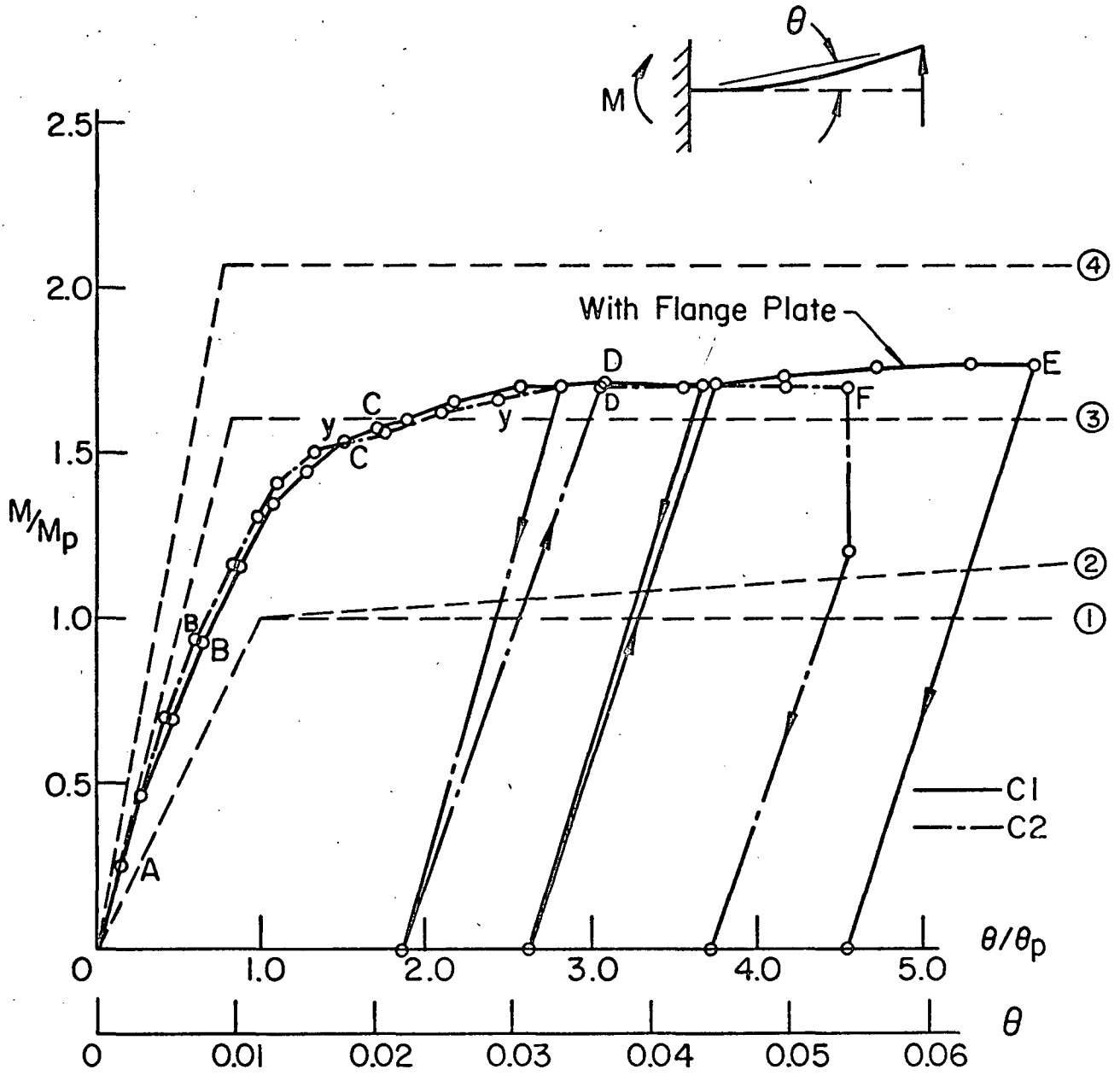

FIG. 20: MOMENT - ROTATION BEHAVIOR : TESTS C1 & C2

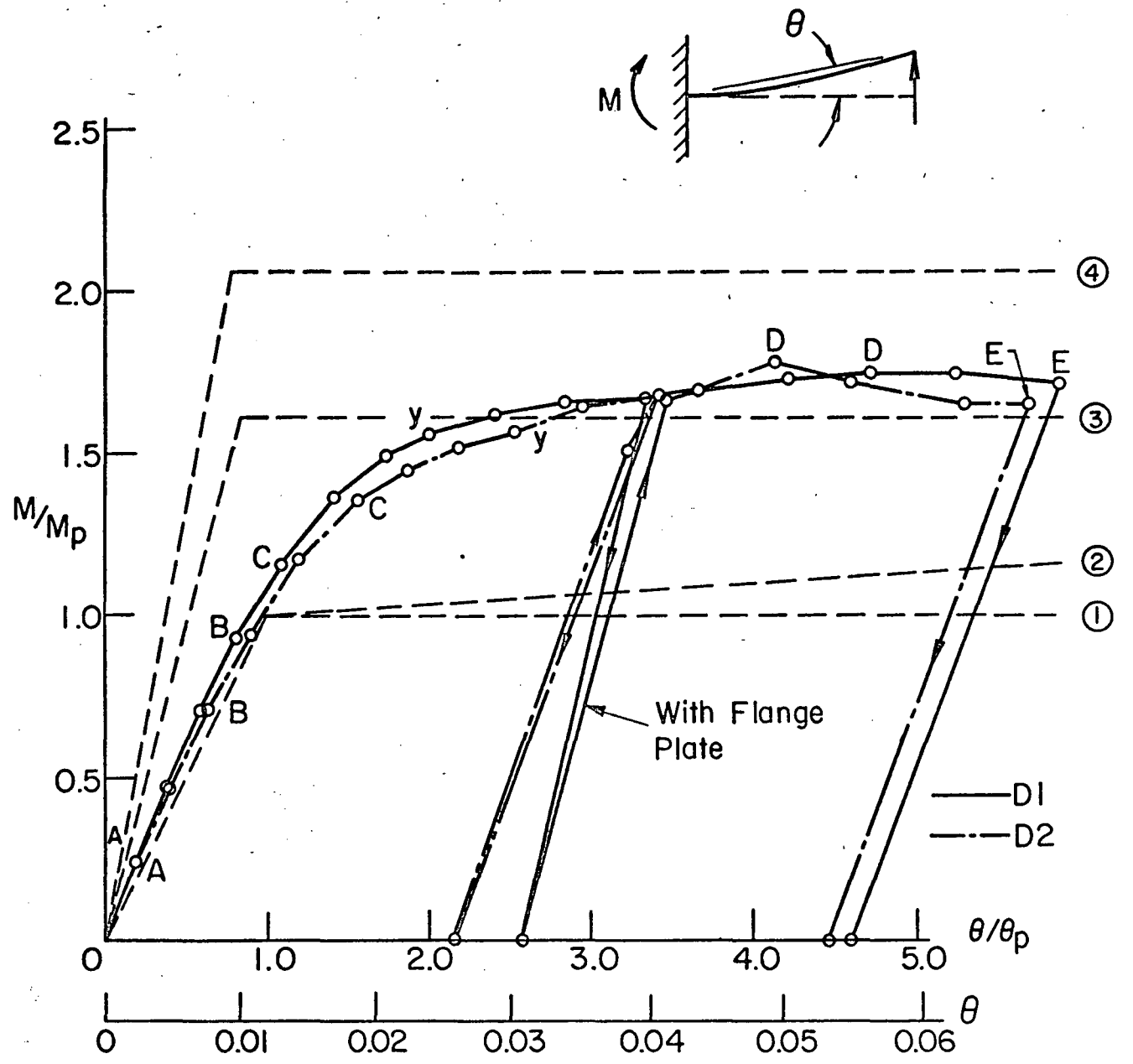

FIG. 21: MOMENT - ROTATION BEHAVIOR : TESTS D1 & D2

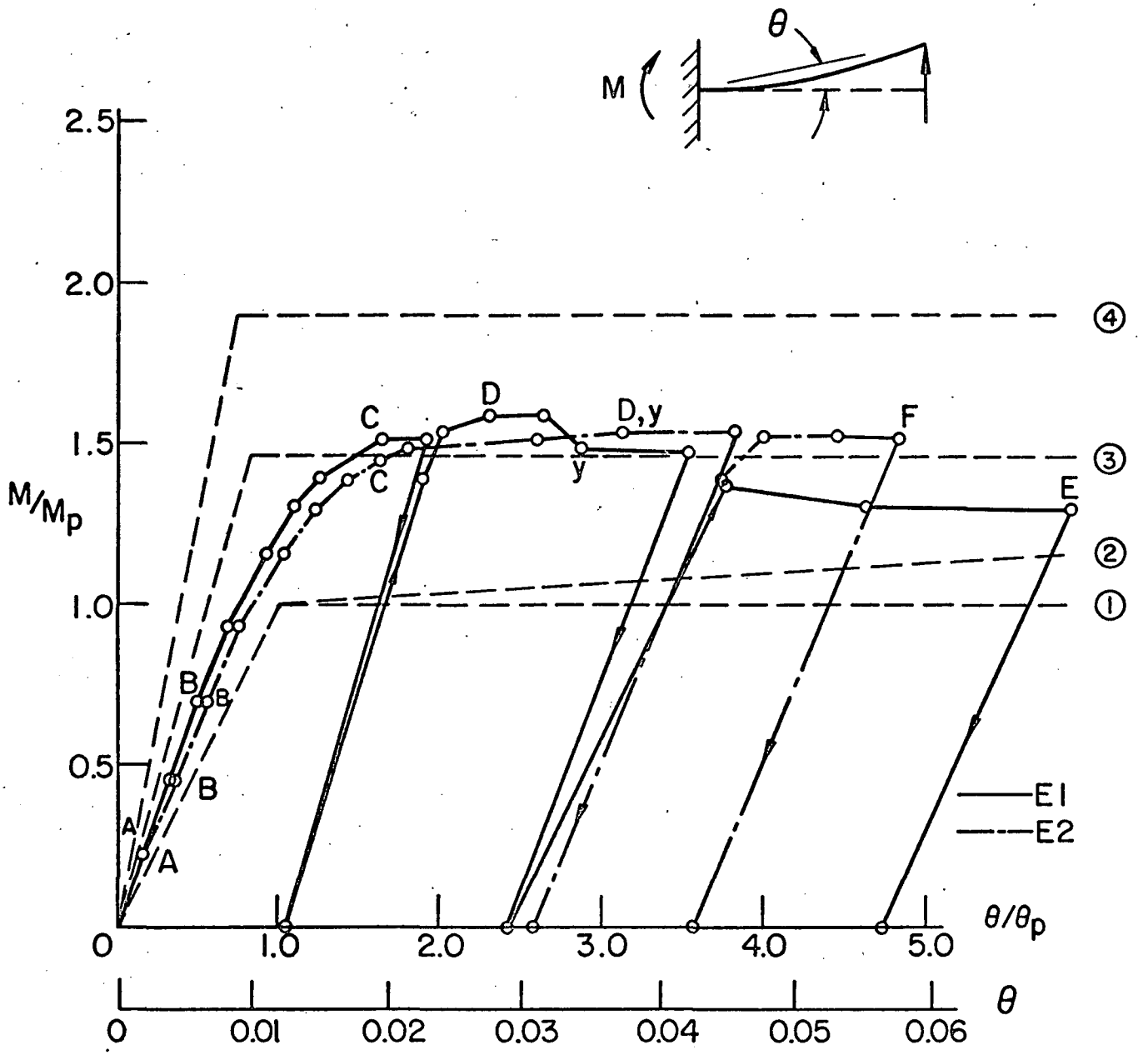

FIG. 22: MOMENT - ROTATION BEHAVIOR : TESTS E1 & E2

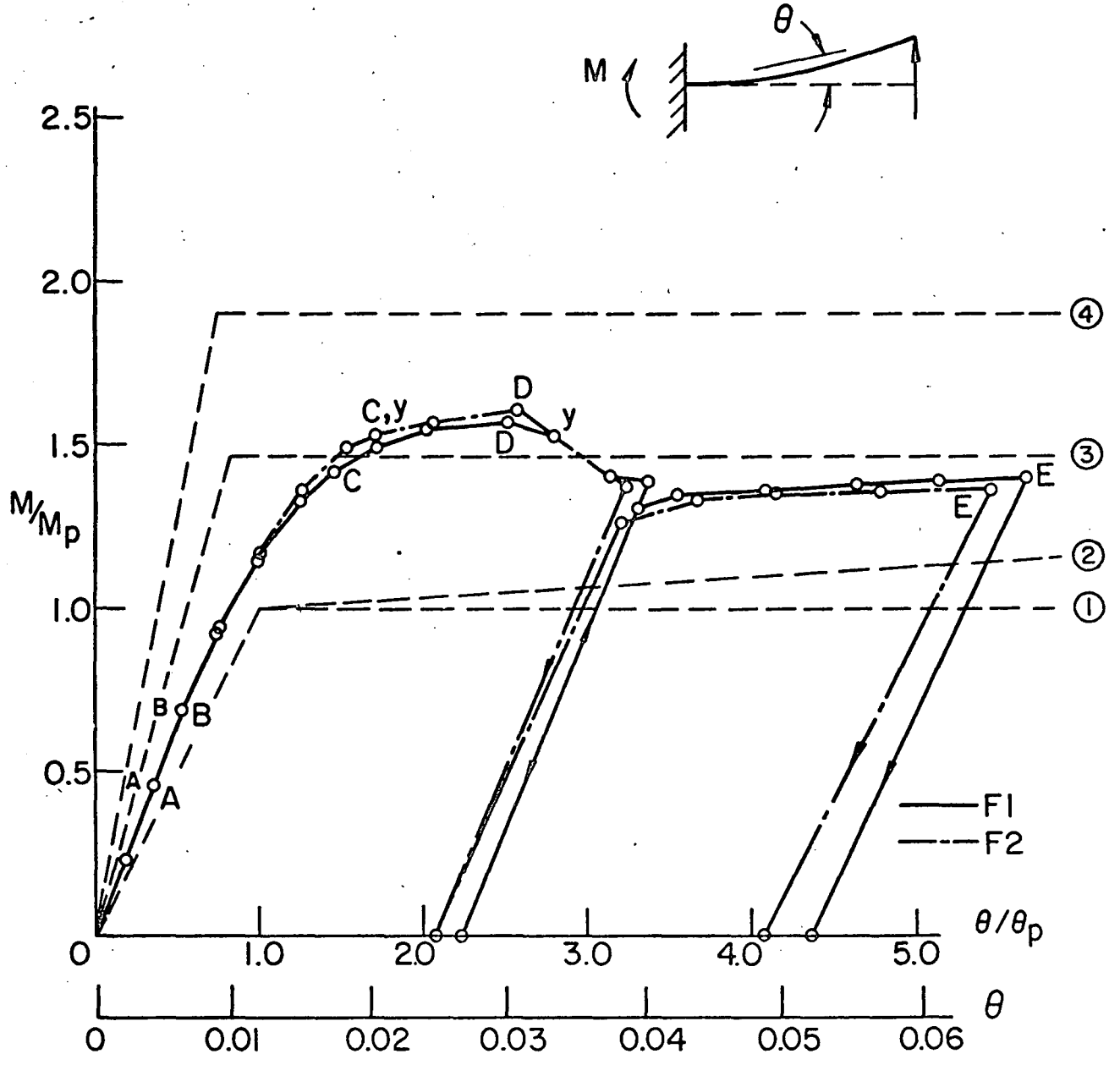

FIG. 23: MOMENT - ROTATION BEHAVIQR : TESTS F1 & F2

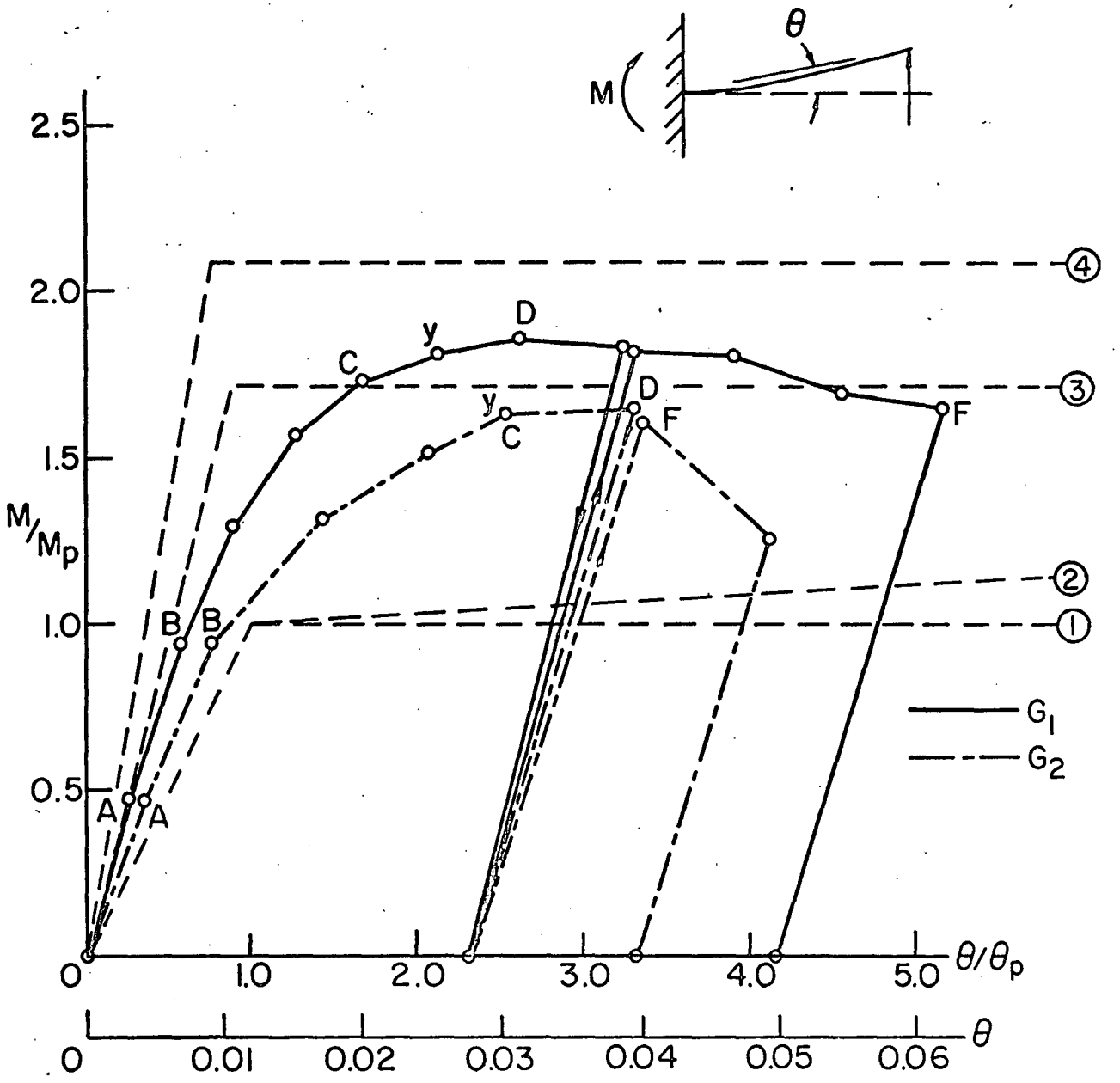

FIG. 24: MOMENT - ROTATION BEHAVIOR : TESTS G1 & G2

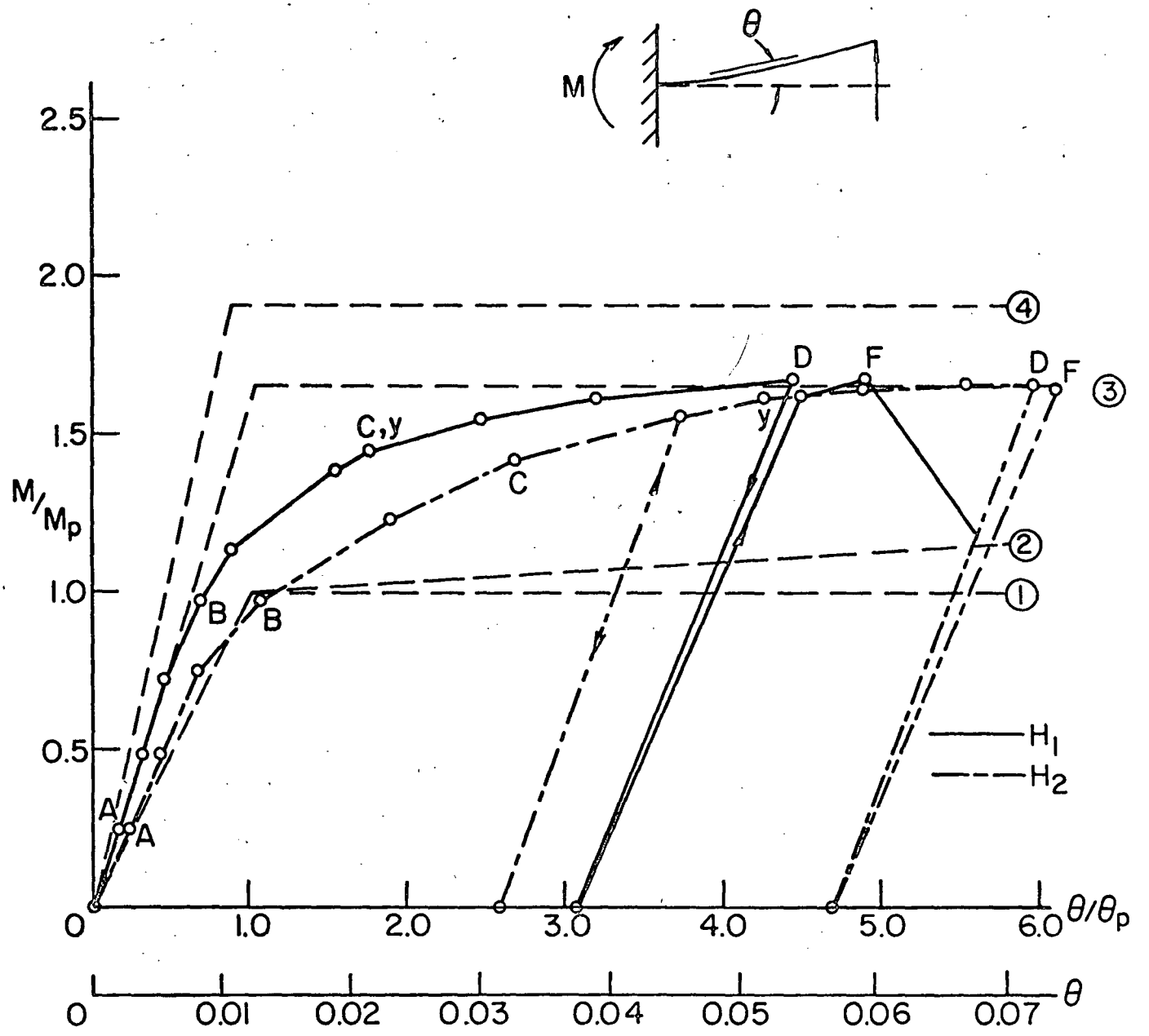

FIG. 25: MOMENT - ROTATION BEHAVIOR : TESTS H1 & H2

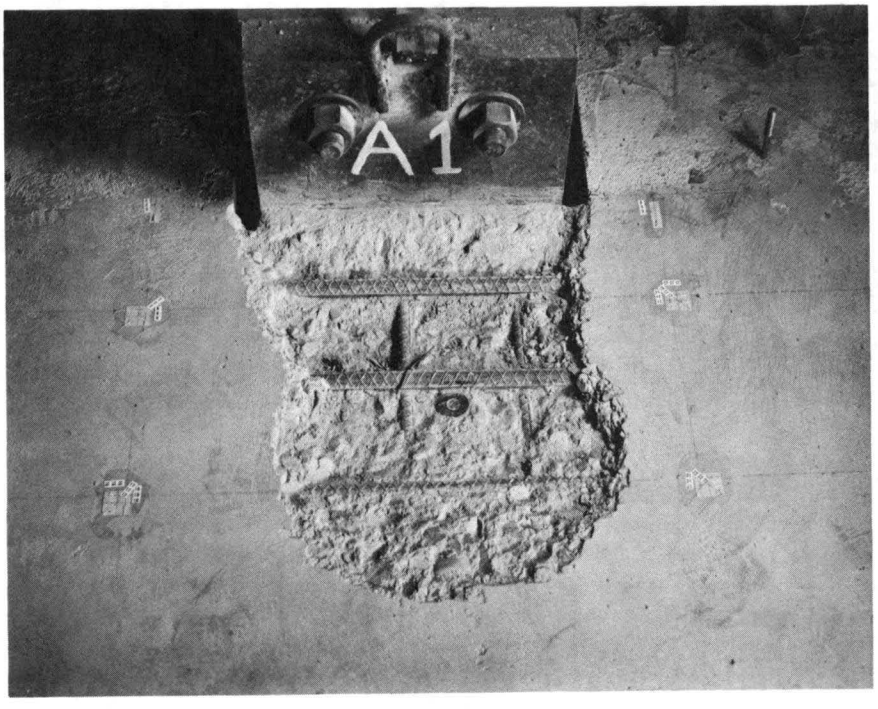

FIG.26a: FAILURE SURFACE OF TEST A1

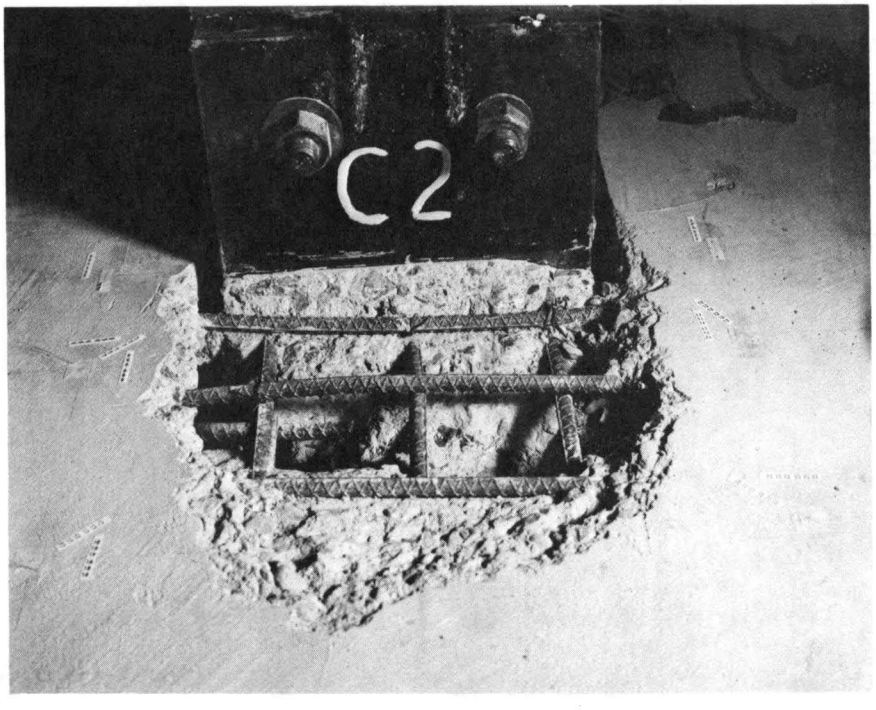

FIG.26b: FAILURE SURFACE OF TEST C2

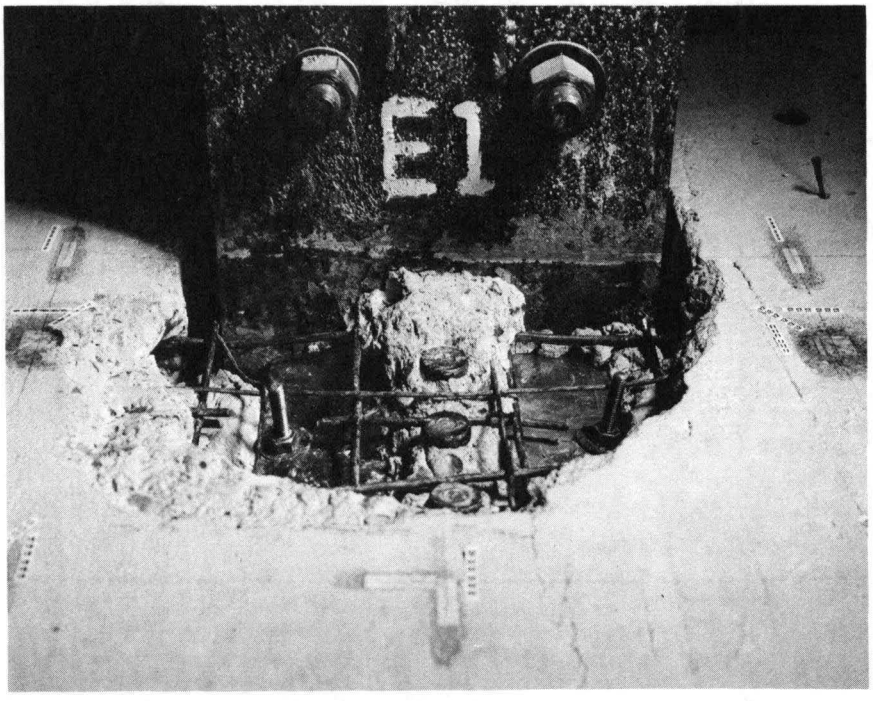

FIG.27a: FAILURE SURFACE OF TEST E1

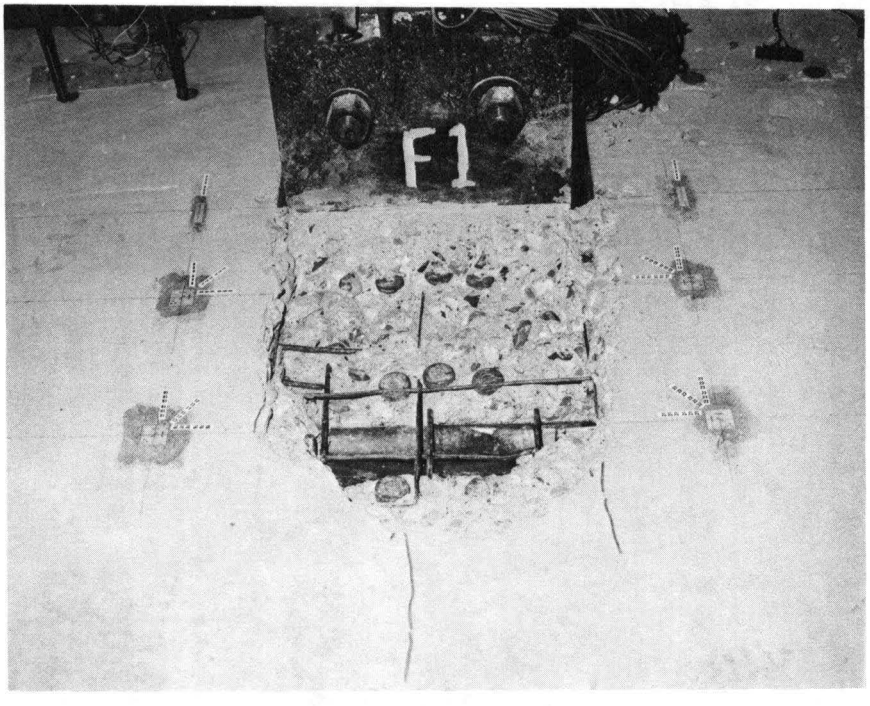

FIG.27b: FAILURE SURFACE OF TEST F1

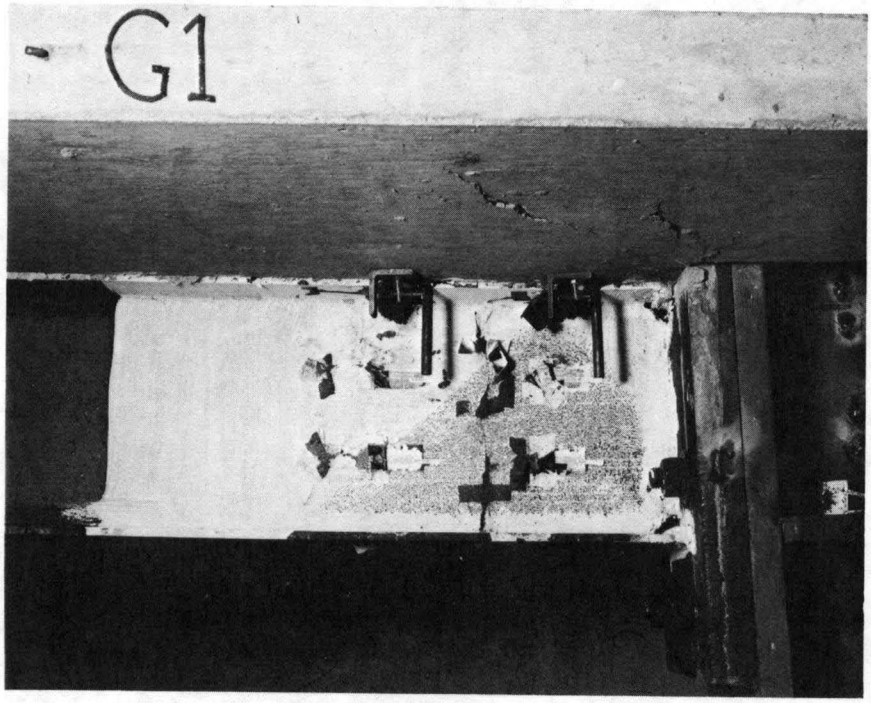

FIG.28a: YIELD PATTERN AND CRACKING OF THE SLAB OF TEST G1

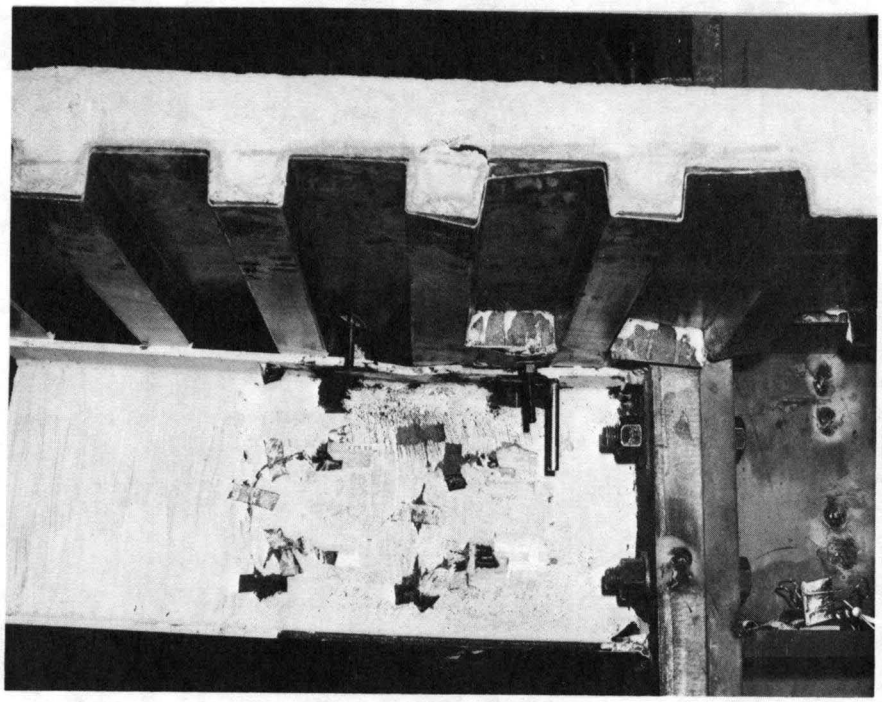

FIG.28b: SHEARING OF THE RIBS AND LOCAL BUCKLING OF THE TOP FLANGE OF TEST F2

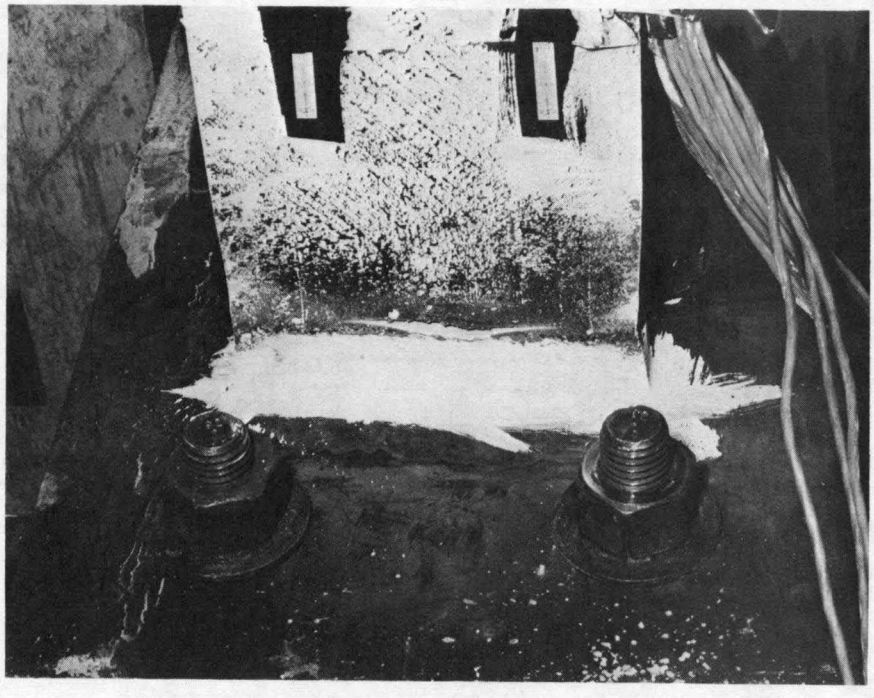

FIG.29a: CRACKING OF THE TENSION FLANGE OF TEST G1

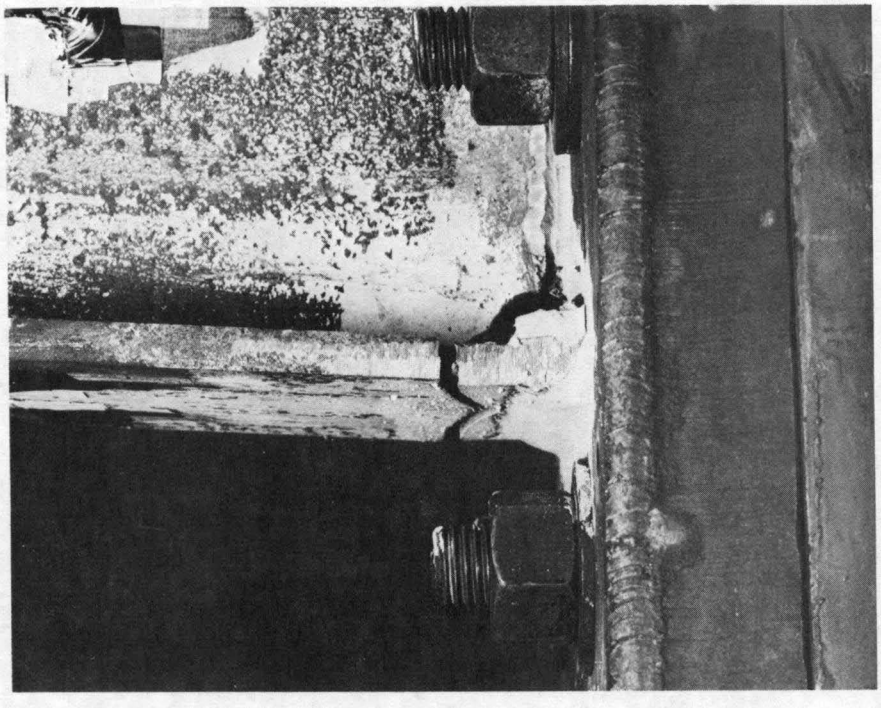

FIG.29b: CRACKING OF THE TENSION FLANGE OF TEST H1

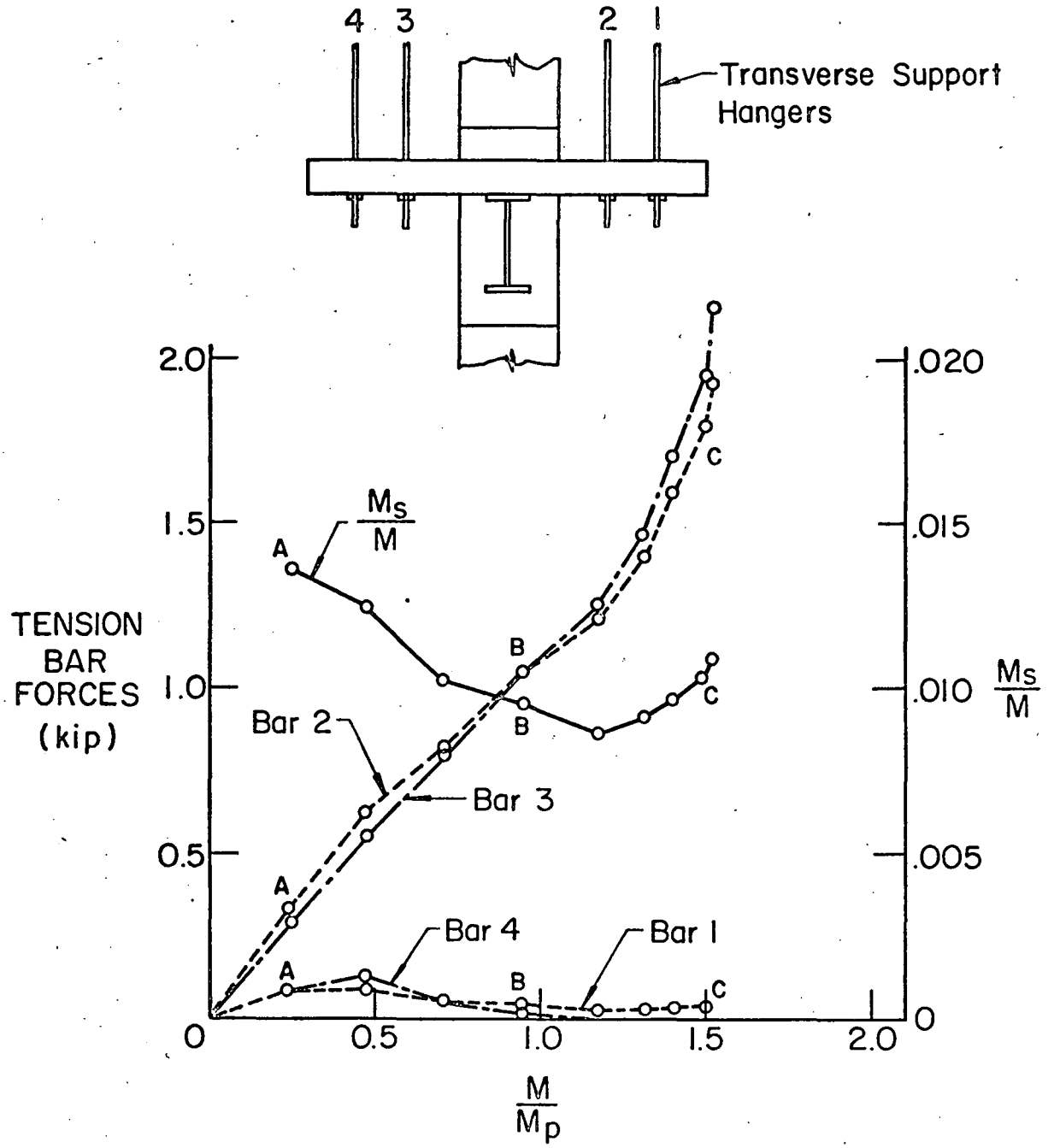

FIG. 30: FORCES IN TRANSVERSE SUPPORT HANGERS OF TEST C2

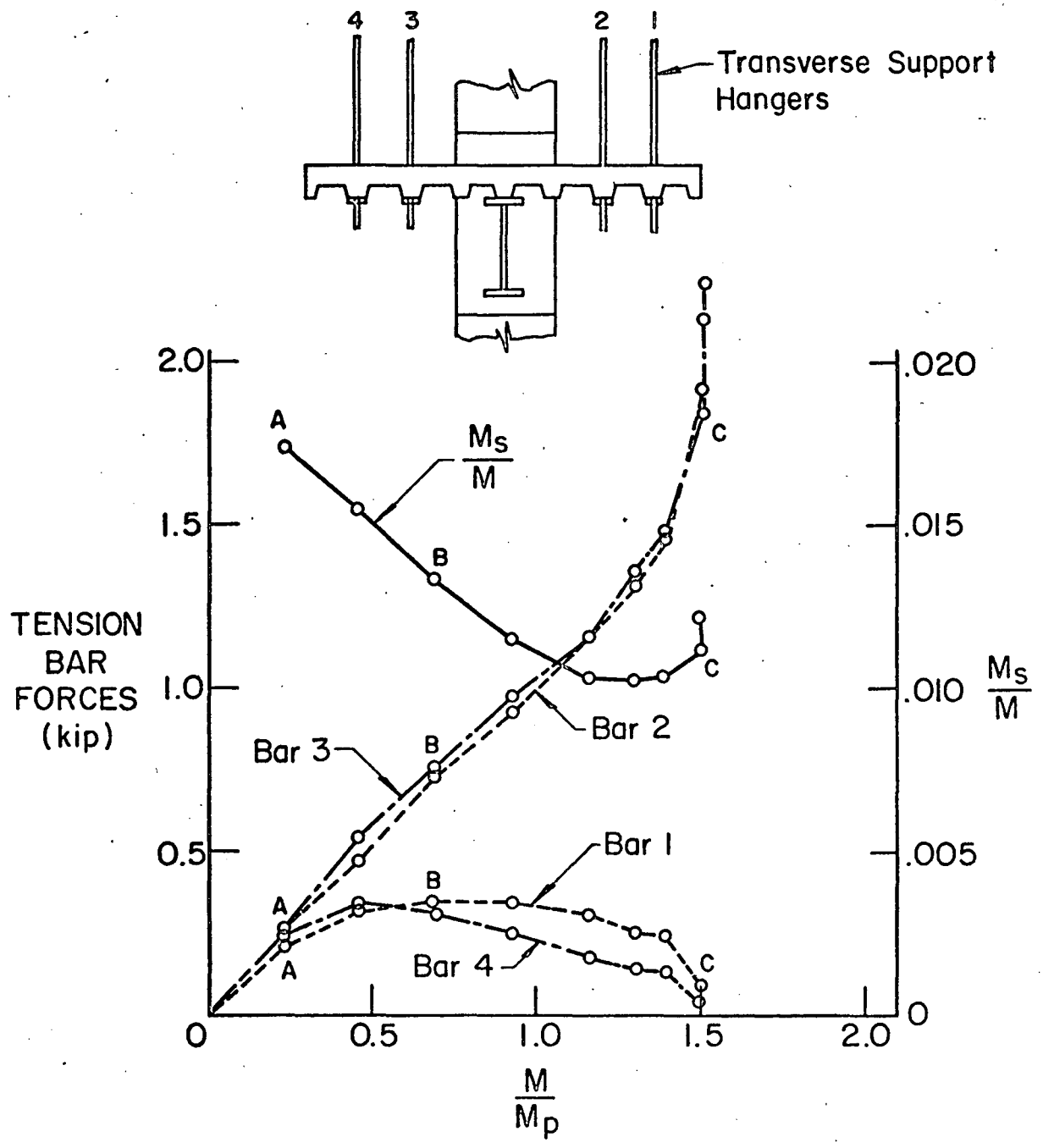

FIG. 31: FORCES IN TRANSVERSE SUPPORT HANGERS OF TEST E1

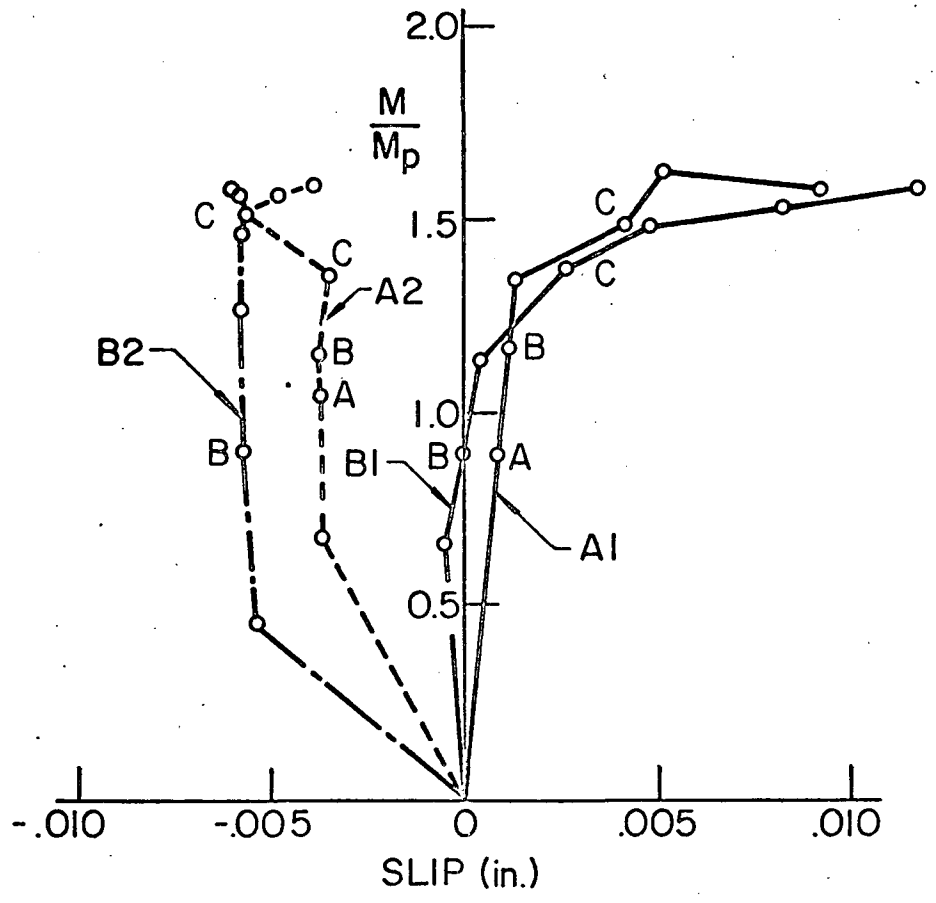

FIG. 32: RELATIVE SLIP BETWEEN SLAB AND STEEL BEAM AT GAGE SECTION B

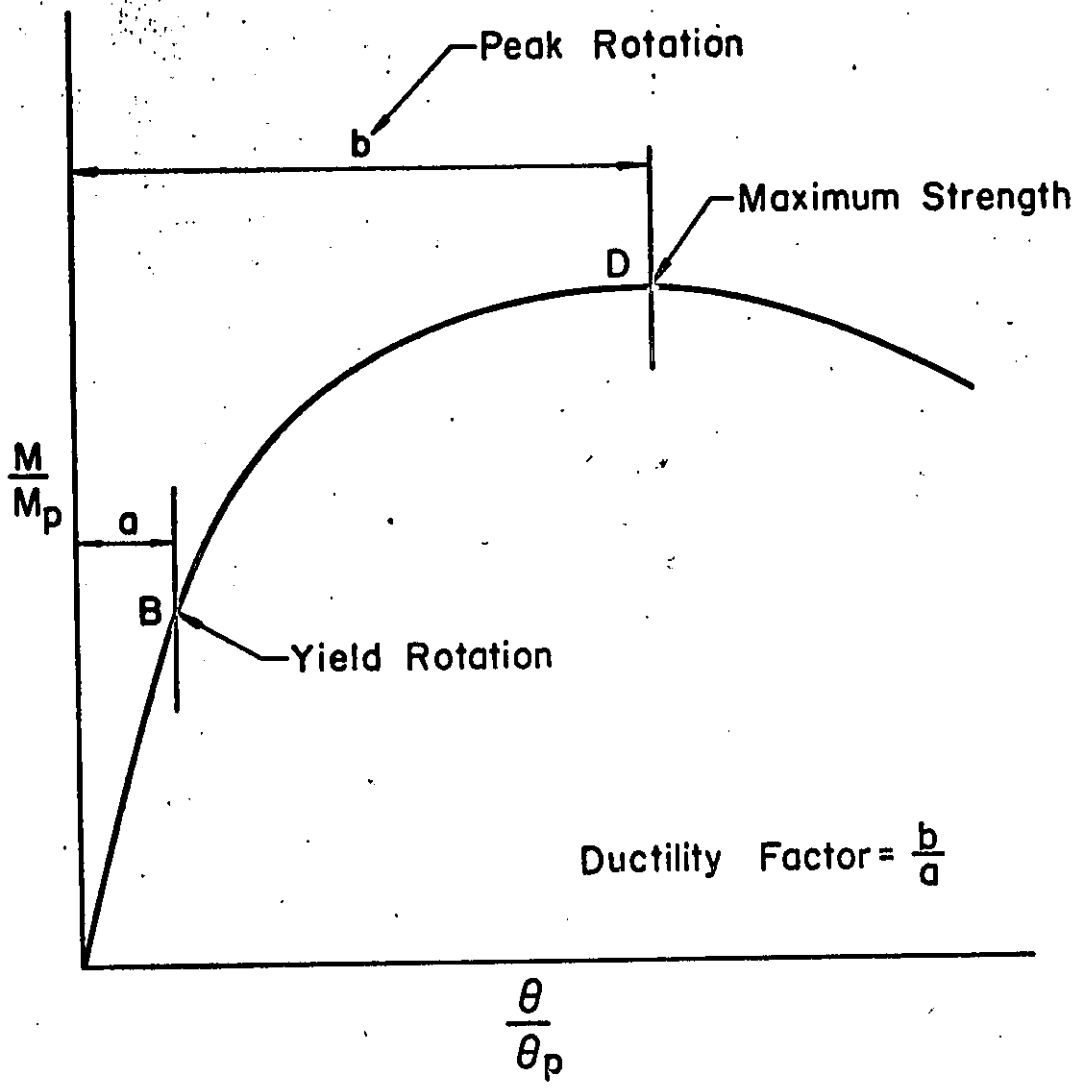

FIG. 33: TYPICAL MOMENT - ROTATION CURVE AND DEFINITION OF DUCTILITY FACTOR

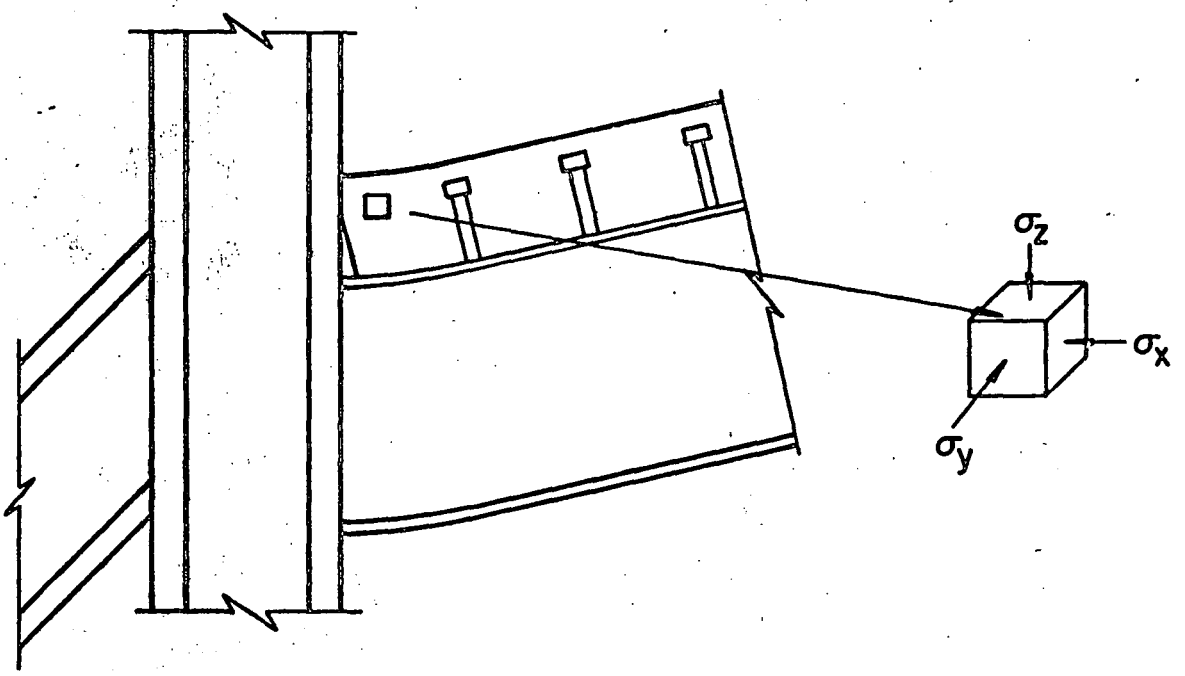

FIG. 34a: THREE SIMENSIONAL STATE OF STRESS IN THE
IN THE PRESENCE OF A SHRINKAGE GAP

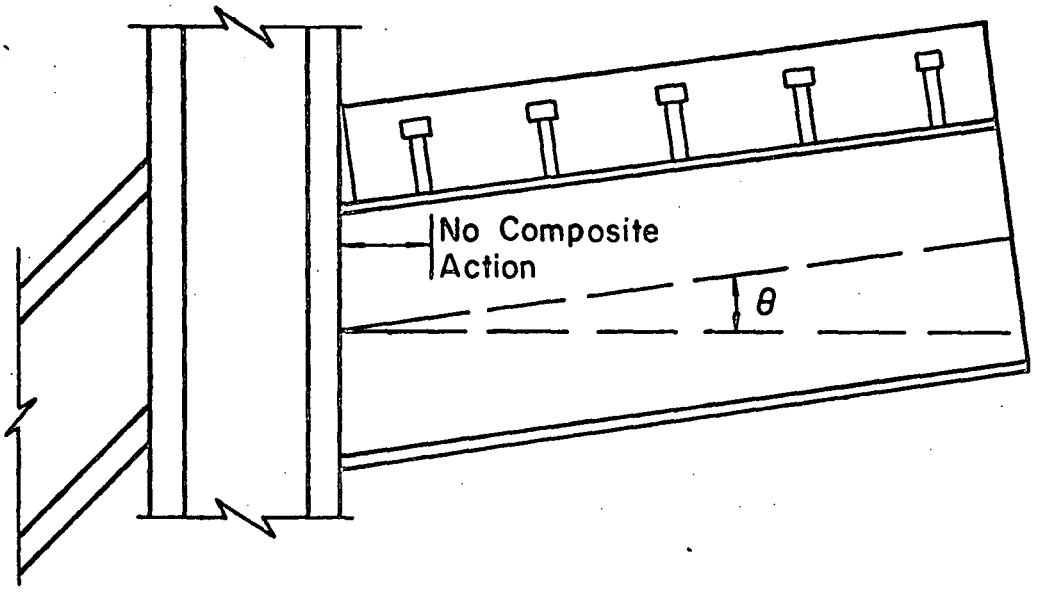

FIG. 34b: ROTATION REQUIRED TO CLOSE SHRINKAGE GAP

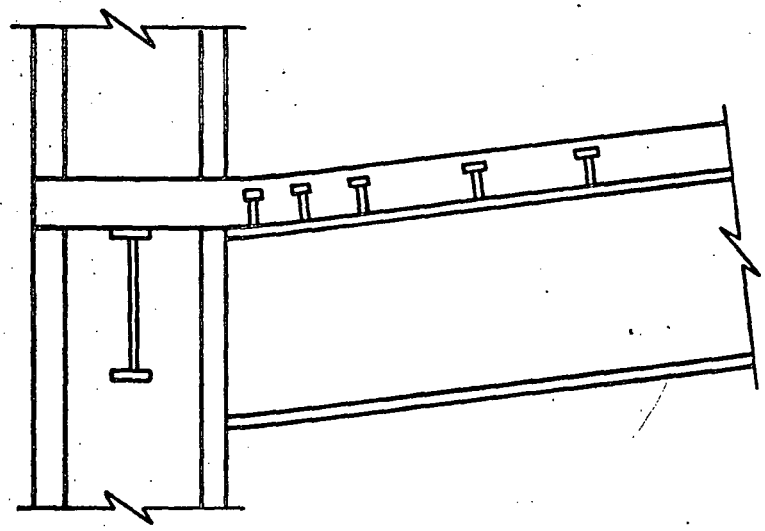

FIG. 35a: DENSE CONNECTOR SPACING AT COLUMN

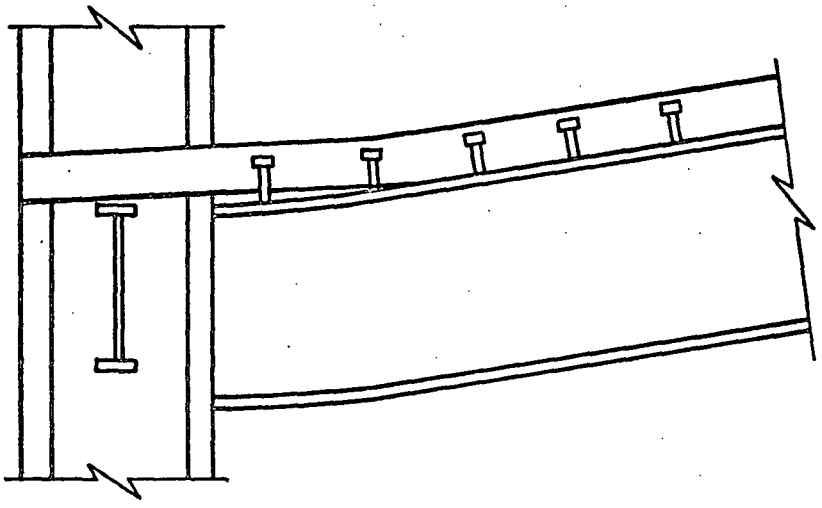

FIG. 35b: NORMAL CONNECTOR SPACING AT COLUMN

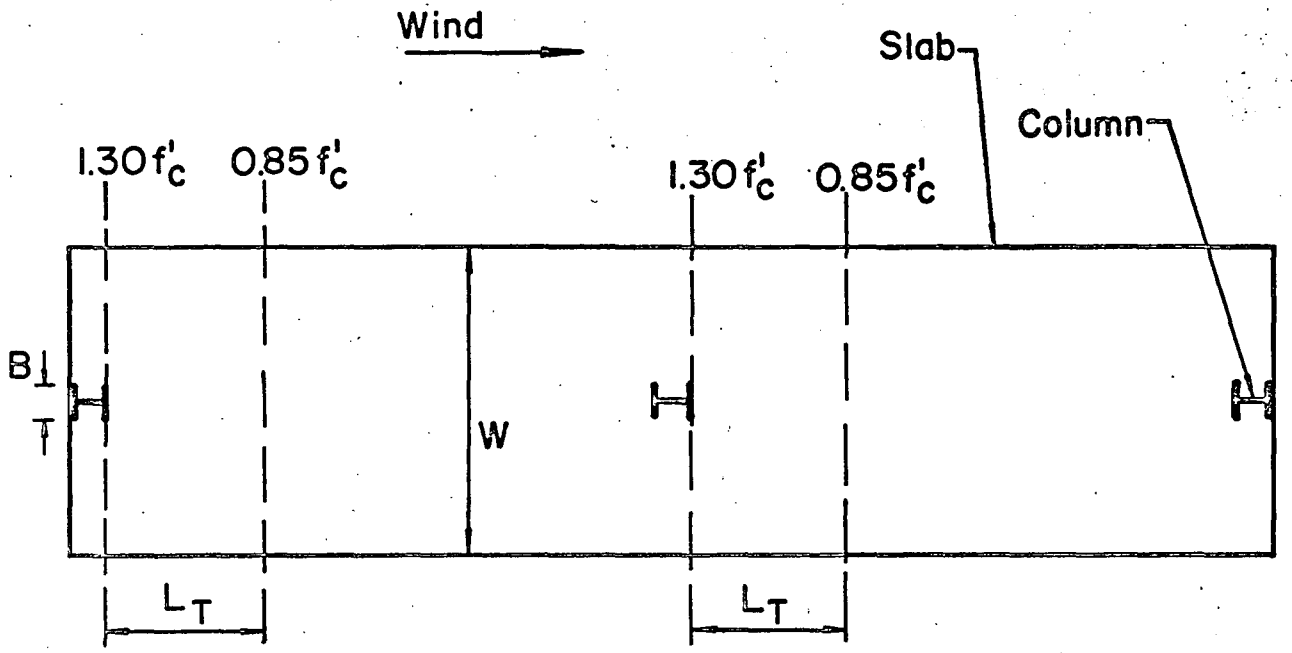

W=Effective Width of Slab

L_T= Transition Length

FIG. 36: PLAN OF UNBRACED FRAME WITH COMPOSITE BEAMS

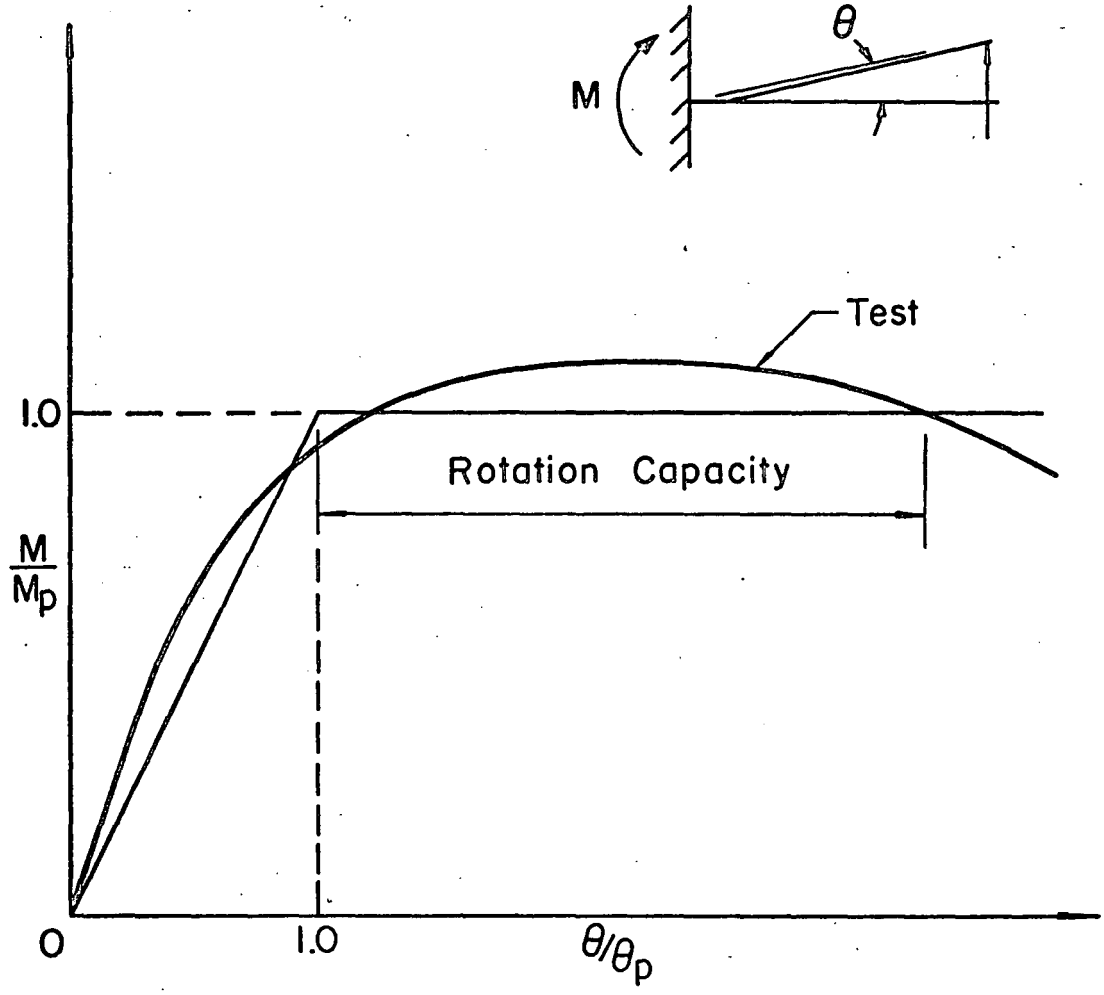

FIG. 37: DEFINITION OF ROTATION CAPACITY

11. REFERENCES

1. El-Dakhakhni, W. M. and Daniels, J. H.
   FRAME-FLOOR-WALL SYSTEM INTERACTION IN BUILDINGS, Fritz Engineering Laboratory Report No. 376.2, Lehigh University, Bethlehem, Pa., April 1973.

2. Daniels, J. H., Kroll, G. D., and Fisher, J. W.
   BEHAVIOR OF COMPOSITE BEAM-TO-COLUMN JOINTS, Journal of the Structural Div., ASCE, Vol. 96, ST3, p. 671, March, 1970.

3. Du Plessis, D. P. and Daniels, J. H.
   EXPERIMENTS ON COMPOSITE BEAMS UNDER POSITIVE END MOMENT, Fritz Engineering Laboratory Report No. 374.2, Lehigh University, Bethlehem, Pa., June 1972.

4. AISC
   SPECIFICATION FOR THE DESIGN, FABRICATION AND ERECTION OF STRUCTURAL STEEL FOR BUILDINGS, February 1969.

5. Kupfer, H., Hilsdorf, H. K. and Rusch, H.
   BEHAVIOR OF CONCRETE UNDER BIAXIAL STRESSES, ACI Journal, Vol. 66, p. 656, August 1969.

6. RESPONSE OF BUILDINGS TO LATERAL FORCES,
   ACI Journal, Vol. 68, p. 81, February, 1971.

7. Sargin, M., Ghosh, S. K. and Handa, V. K.
   EFFECTS OF LATERAL REINFORCEMENT UPON THE STRENGTH AND DEFORMATION PROPERTIES OF CONCRETE, Magazine of Concrete Research, Vol. 23, No. 75-76, p. 99, June-September, 1971.

8. Iyengar, K. T. S. R., Desayi, P. and Reddy, C. N.
   STRESS-STRAIN CHARACTERISTICS OF CONCRETE CONFINED IN STEEL BINDERS, Magazine of Concrete Research, Vol. 22, No. 72, p. 173, September 1970.

9. Du Plessis, D. P.
   ANALYSIS OF UNBRACED FRAMES WITH COMPOSITE FLOORS, Dissertation to be presented to the Dept. of Civil Engineering, Lehigh University, Bethlehem, Pa., in partial fullfillment of the requirements for the degree of Doctor of Philosophy.

10. Beedle, L. S.
    PLASTIC DESIGN OF STEEL FRAMES, John Wiley & Sons, Inc., 1958.

11. ASCE Manual 41;
    PLASTIC DESIGN IN STEEL, A Guide and Commentary, 1971.